2mi4

NASA CR-134170
ERIM 31650-75-T

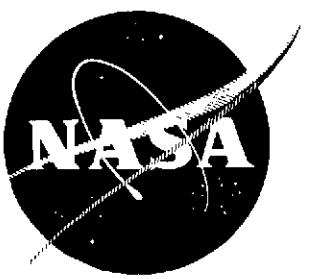

DISCRIMINATION TECHNIQUES EMPLOYING BOTH REFLECTIVE AND THERMAL MULTISPECTRAL SIGNALS

by

W. A. Malila, R. B. Crane, and W. Richardson
INFRARED AND OPTICS DIVISION

prepared for

NATIONAL AERONAUTICS AND SPACE ADMINISTRATION

Johnson Space Center, Houston, Texas 77058
Earth Observations Division
NAS 9-9784

NOTICES

Sponsorship. The work reported herein was conducted by the Environmental Research Institute of Michigan for the National Aeronautics and Space Administration, Johnson Space Center under Contract NAS 9-9784, Task C1. Dr. Andrew Potter (TF3) is Technical Monitor. Contracts and grants to the Institute for the support of sponsored research are administered through the Office of Contracts Administration.

Disclaimers. This report was prepared as an account of Government-sponsored work. Neither the United States, nor the National Aeronautics and Space Administration (NASA), nor any person acting on behalf of NASA:

(A) Makes any warranty or representation, expressed or implied with respect to the accuracy, completeness, or usefulness of the information contained in this report, or that the use of any information, apparatus, method, or process disclosed in this report may not infringe privately owned rights; or

(B) Assumes any liabilities with respect to the use of, or for damages resulting from the use of any information, apparatus, method, or process disclosed in this report.

As used above, "person acting on behalf of NASA" includes any employee or contractor of NASA, or employee of such contractor, to the extent that such employee or contractor of NASA or employee of such contractor prepares, disseminates, or provides access to any information pursuant to his employment or contract with NASA, or his employment with such contractor.

Availability Notice. Requests for copies of this report should be referred to:

National Aeronautics and Space Administration
Scientific and Technical Information Facility
P. O. Box 33
College Park, Maryland 20740

Final Disposition. After this document has served its purpose, it may be destroyed. Please do not return it to the Environmental Research Institute of Michigan.

TECHNICAL REPORT STANDARD TITLE PAGE

1. Report No.	2. Government Accession No.	3. Recipient's Catalog No.
NASA-CR-		

4. Title and Subtitle	5. Report Date
DISCRIMINATION TECHNIQUES EMPLOYING BOTH REFLECTIVE AND THERMAL MULTISPECTRAL SIGNALS	November 1973
	6. Performing Organization Code
7. Author(s)	8. Performing Organization Report No.
W. A. Malila, R. B. Crane, and W. Richardson	ERIM 31650-75-T
9. Performing Organization Name and Address	10. Work Unit No.
Environmental Research Institute of Michigan P.O. Box 618 Ann Arbor, Michigan 48107	Task C1
	11. Contract or Grant No.
	NAS9-9784
	13. Type of Report and Period Covered
12. Sponsoring Agency Name and Address	Technical Report 11 Nov. 1971-31 Jan. 1973
National Aeronautics and Space Administration Johnson Space Center, Houston, Texas 77058	14. Sponsoring Agency Code

15. Supplementary Notes

Dr. Andrew Potter (TF3) is the NASA/JSC Technical Monitor

16. Abstract

Recent improvements in remote sensor technology carry implications for data processing. Multispectral line scanners now exist that can collect data simultaneously and in registration in multiple channels at both reflective and thermal (emissive) wavelengths. Progress in dealing with two resultant recognition processing problems is discussed. (1) More channels mean higher processing costs; to combat these costs, a new and faster procedure for selecting subsets of channels has been developed. (2) Differences between thermal and reflective characteristics influence recognition processing; to illustrate the magnitude of these differences, some explanatory calculations are presented. Also introduced, is a different way to process multispectral scanner data—namely, radiation balance mapping and related procedures. Techniques and potentials are discussed and examples presented.

17. Key Words	18. Distribution Statement
Remote sensor technology, Multispectral data collection, Recognition processing, Radiation balance mapping, Energy budget, Soil temperatures, Channel selection criteria	

19. Security Classif. (of this report)	20. Security Classif. (of this page)	21. No. of Pages	22. Price
UNCLASSIFIED	(U)	~~vi + 47~~ 50	4.75

FOREWORD

This report describes part of a comprehensive and continuing program of research in multispectral remote sensing of environment from aircraft and satellites. The research is being carried out for NASA's Johnson Space Center, Houston, Texas, by the Environmental Research Institute of Michigan (ERIM), formerly the Willow Run Laboratories, a unit of The University of Michigan's Institute of Science and Technology. Dr. Andrew Potter is the NASA/JSC Technical Monitor. The basic objective of this program is to develop remote sensing as a practical tool for obtaining extensive information quickly and economically.

The reported work was performed under Contract NAS 9-9784, Task C1. Contractor personnel responsible for program direction are R. R. Legault, a Director of the Environmental Research Institute of Michigan, and J. D. Erickson, Principal Investigator and Head of the ERIM Information Systems and Analysis Section. Mr. William A. Malila served as Task Leader and author of Sections 4 and 5. The work reported in Section 3 was performed primarily by Dr. Robert B. Crane and Dr. Wyman Richardson. The assistance of Mr. Robert Horvath in making the thermal calculations of Section 4 is acknowledged, as are the computer programming efforts of Mr. David Zuk and the assistance and analysis of Mr. Jackson P. Livisay for the work reported in Section 5. Dr. Gene Safir, Michigan State University, provided field observation notes describing natural features of the agricultural tract studied in Section 5.

This report was submitted for sponsor approval on 1 February 1973.

CONTENTS

PRECEDING PAGE BLANK NOT FILMED

FIGURES

DISCRIMINATION TECHNIQUES EMPLOYING BOTH REFLECTIVE AND THERMAL MULTISPECTRAL SIGNALS

1

SUMMARY

The M-7 multispectral scanner—at that time operated by the Willow Run Laboratories—collected data simultaneously and in registration in both reflective and thermal (emissive) wavelength intervals for the Corn Blight Watch Experiment during the summer of 1971; now ERIM-owned, the M-7 retains this capability. (With the previous M-5 scanner, thermal data were not in registration with reflective data.) Similarly, the new 24-channel multispectral data system (MSDS) scanner, delivered to NASA by the Bendix Corporation, has the capability of collecting data in several emissive channels in registration with data in reflective channels.

New multispectral data collection capabilities present both problems for recognition processing and opportunities for new and improved techniques; both aspects are discussed in this report.

One problem in recognition processing is that costs are high when many information channels are used; therefore, to cut such costs, an improved method was developed for reducing the number of channels used. The number of information channels can be reduced either by combining signals from two or more channels or by the judicious selection of subsets of channels for processing. The present report discusses and describes channel selection procedures in which we use the Bayesian criterion—average expected loss—as a performance measure. This criterion can be formulated as an average probability of misclassification which can easily be understood and interpreted. As compared to our former procedure which employed an accurate but time-consuming quadratic calculation of the probability of misclassification, our new procedure, which is based on a linear approximation, yields comparable results in 1/50th of the computation time.

Another problem (and opportunity) stems from the fact that the thermal and reflective signals are produced by different physical mechanisms. This has implications for the ways in which signatures vary under changing conditions of observation and measurement, and for the variability present under fixed conditions. The problem of cloud shadows is discussed and calculations with a thermal model then presented to show that a one-hour late-morning cloud shadow can reduce the temperature of a typical bare-soil patch throughout the remainder of the day, by from 2 to 21°F below that of the same or similar soil without a shadow. Vegetation responds much more quickly to the presence or removal of a cloud shadow and hence would exhibit a lesser residual effect.

A different method for processing multispectral scanner data is also introduced. Called radiation-balance mapping, it takes advantage of the simultaneity of reflective and thermal data.

The exitance (total outgoing radiation) of a surface is estimated by a weighted sum of multispectral scanner signals calibrated in terms of radiance. Scene exitance maps then can be produced. By then estimating the incoming irradiance, the instantaneous radiation balances of surfaces can be estimated and also mapped. These radiation balance quantities have potential for use in the quantitative interpretation of scene material conditions. Examples of both types of maps are presented for agricultural and urban applications.

In related work, a recognition processing procedure was developed whereby a function of the input signals (here it might be the linear combination that represents the exitance) is produced as a second channel of output data along with the recognition output. A histogram of the function values for each recognition class is also produced. A companion printout display program prints a gray-scale map of the data in one output channel when the data in the other channel meet a specified criterion; thus, for example, one could make a map showing the exitance values for all data points recognized as corn.

2
INTRODUCTION

Remote sensing technology has been, and is being, successfully applied toward the solution of various Earth Resources survey, analysis, and management problems. For example, aerial photography has been utilized for several decades in studying forestry, agriculture, soils, range and wildlife management, geology, hydrology, and engineering problems [1]. In recent years other types of remote sensing instruments such as television cameras and optical/mechanical scanners have been introduced. This report deals primarily with the processing and analysis of data from optical/mechanical scanners, particularly multispectral line scanners.

A multispectral scanner features a number of different detectors that simultaneously sense radiation propagated in different spectral regions from a common ground-resolution element. Data from each detector channel are recorded on separate magnetic tape channels for subsequent playback and analysis in either image or nonimage form. Imagery can be interpreted manually by using techniques similar to those employed in photointerpretation. In addition, the recorded data are in a form amenable to processing and analysis with special-purpose and general-purpose computers of both analog and digital type. Much work has been performed over the past several years on the development, testing, and use of computer processing techniques for recognition mapping with multispectral scanner data.

The Environmental Research Institute of Michigan (formerly Willow Run Laboratories of The University of Michigan) began flying a multispectral scanner system in the early 1960's. The first scanner with truly simultaneous data collection (in 12 channels) was flown by the WRL beginning in 1966 [2]. It covered the spectral region 0.4 to 1.0 μm, and was accompanied by another scanner which obtained near-simultaneous coverage at thermal-infrared and other wavelengths. However, problems in spatially registering the thermal data of the one scanner with the multichannel data of the other unfortunately precluded most joint processing of the thermal (emissive) data and the multichannel reflective data. Then in 1971, the Michigan M-7 scanner was developed and flown operationally during the Corn Blight Watch Experiment, June through September, 1971. The M-7 scanner has a thermal channel in spatial registration with the visible and near-infrared channels [3]. Later in 1971, the 24-channel multispectral scanner system (MSDS) fabricated for NASA by the Bendix Aerospace Systems Division was flight tested and delivered. Both the M-7 and MSDS systems put thermal data in synchronism with reflective data, so joint processing of these data is a timely topic. Two aspects of such joint processing are discussed in this report: recognition mapping and radiation-balance mapping.

A straightforward way to use data in the thermal channel(s) for recognition processing is to treat these data no differently than reflective data—that is, treat them as just one or more additional channels from which to extract signatures representing the various classes of material in the scene; establish decision rules for classification; and apply these rules to all data points in the scene. Such a procedure actually was followed in the recognition processing of data for the Corn Blight Watch Experiment.

Two problems in recognition processing are introduced by additional channels. The first is the larger number of channels available with attendant increases in processing cost; the second is the different nature of thermal signatures for materials as compared to reflective signatures for the same materials.

The number of information channels used for recognition processing can be reduced by linearly combining channels or by selecting subsets of channels. Without significant reduction in performance, a proper reduction of information channels for recognition processing can reduce digital processing costs (which equate with computing times and are proportional to the square of the number of channels for the usual quadratic decision rules when implemented on a general-purpose digital computer), and/or can increase the number of material classes that can be handled by special-purpose computers such as the Michigan parallel analog processor, SPARC (SPectral Analysis and Recognition Computer). (SPARC's overall capacity limit, based on number of classes times number of information channels, is ≤ 48.) To date, the most common method of reducing the number of information channels has been to select subsets of the available data channels. The thermal channel was frequently among the 6 selected from the 12 channels available for processing Corn-Blight-Watch (CBW) data. Subsequent to the CBW experiment, we developed an improved (faster) digital technique for selecting subsets of channels. This technique, first reported in Ref. [4] and currently reviewed in Section 3, makes use of a linear approximation to the quadratic calculation of probability of misclassification. (References [5] and [6] describe a further development of the linear technique that has been applied in recognition algorithms themselves.)

The other recognition processing problem introduced by the thermal channel(s) occurs because a thermal signal results from different physical processes than does a reflective signal. (As discussed in Section 4, a thermal signal results from self-emission that depends on the temperature and emittance of the material, whereas a reflective signal depends on the incident radiation and the reflectance characteristics of the material.) This difference in the origin of thermal signals lends attributes that can at times cause misclassifications of materials, but at other times may improve discrimination. For example, consider a clear-sky situation. The temperature of a material on the ground depends on physiological, physical, and meteorological

factors often having little, if any, influence on the reflectance of the material. Also, the temperature depends not only on the existing environmental conditions but also to an extent on the past history of such conditions. Thus two fields of a given crop might be recognized as belonging to the same class if reflective signatures were used, but if thermal data were added to the decision procedure, one field might differ thermally and be classified differently. The response of surface materials to the passing of cloud shadows is also different in the two spectral regions. Finally, the way in which signatures change with time and distance from the training data will differ in the two spectral regions because of the different physical processes involved.

One can take advantage of these differences between reflective and thermal data by using them jointly for quantitative interpretation of surface material conditions. For example, a surface material's condition influences its radiation balance and energy budget; so a weighted linear combination of multispectral scanner signals can be used to estimate the radiant exitance of the surface, that is, to estimate the total outgoing radiation at both reflective and thermal wavelengths. The exitance is a principal component of the instantaneous radiation balance of the surface. In turn, radiation balance is a major factor in the energy budget of the surface (another factor is heat loss by evapotranspiration). In the example of the two fields of a given crop, the thermal difference between the two might have been caused by different amounts of evapotranspiration: one field with a plentiful supply of water, the other approaching a moisture-stress condition. Procedures for creating exitance maps and radiation balance maps of surface areas are introduced and discussed in Section 5 of this report and some first examples of such maps presented; revised recognition processing and display programs that incorporate new features based on our current studies are also discussed therein.

3
PROCEDURES FOR SELECTING SUBSETS OF CHANNELS

3.1. GENERAL

In recognition processing—which requires numerous calculations of quadratic likelihood—overall cost is directly proportional to the square of the number of channels used.* If these calculations are made by general-purpose digital means, the cost is in computer run time. If, on the other hand, special-purpose methods are employed, the processing cost will lie in quantity of equipment required or, as an alternate penalty, in reduced numbers of material classes that can be included in a given implementation. By carefully selecting subsets of channels, however, processing costs can be reduced without appreciable performance sacrifice. The channel selection methods discussed below have been implemented on a digital computer.

3.2. CRITERION FOR CHANNEL SELECTION

In order to choose subsets of channels, it is necessary to have a criterion for doing so. We prefer the Bayesian criterion of average expected loss (which can be formulated as an average probability of misclassification) for both performance evaluation and channel selection. Allowing direct physical interpretation, it can be applied when the objective is to optimize performance either in choosing between a few material classes in a scene or between all material classes.

In the context of multispectral recognition, the average expected loss is defined as follows. Let us suppose that a decision is being made as to which of K materials is to be observed. You specify in advance a rule for making this decision; we have been using, for example, the maximum likelihood rule that the material chosen is the one with the largest normal likelihood function. Let p_{ij} be the probability that the rule will choose material i, given that the material really is j. If 1_{ij} is a cost factor that measures how much you lose by making this erroneous decision, then

$$L_j = \sum_{i=1}^{K} p_{ij} 1_{ij} \tag{1}$$

is the loss expected to be incurred when material j is observed.

*The current ERIM M-7 multispectral scanner typically collects and records data in 12 spectral channels, and the new NASA/Bendix multispectral scanner (MSDS) is a 24-channel device.

It is not possible to construct a rule for minimizing all of the losses, $L_1, L_2, \ldots, L_K$, simultaneously. For example, L_1 would be minimized by using the rule "always choose material 1," but then $L_2, \ldots, L_K$ all would be maximized. Bayesian theory strikes a balance between these expected losses by minimizing a weighted average of them, that is,

$$L = w_1 L_1 + w_2 L_2 + \ldots w_K L_K = \sum_{j=1}^{K} w_j L_j \tag{2}$$

$$= \sum_{j=1}^{K} \sum_{i=1}^{K} w_j 1_{ij} p_{ij} \tag{3}$$

The rule that accomplishes this minimization is called the Bayesian decision rule.

The weights, w_j, can be interpreted as prior probabilities of the K materials. For suppose that there were a chance mechanism for assigning materials to resolution elements and w_j were the probability that material j would be assigned to the resolution element, then

$$\sum_{j=1}^{K} w_j L_j$$

would be the total expected loss, which the decision maker would seek to minimize. Thus, when weights, w_j, are specified in a Bayesian decision rule, the decision maker is in effect estimating the prior probabilities of the materials. A conventional procedure when the prior probabilities are not known is to make the weights equal, i.e., $w_j = \frac{1}{K}$, so

$$L = \frac{1}{K} \sum_{j=1}^{K} L_j = \frac{1}{K} \sum_{j=1}^{K} \sum_{i=1}^{K} p_{ij} 1_{ij}$$

If the losses are also assumed equal (except $1_{ii} = 0$), it can be shown that the Bayesian decision rule is the same as the maximum likelihood decision rule.

Ideally, then, questions about channel selection are answered by computing the average expected loss. The best subset of size s is the one that produces the smallest average expected loss. If one were to find the best subset of size 1, the best subset of size 2, and so on for all $s \leq N$, where N is the number of channels available, the average expected loss for each subset then would be a decreasing function of s. By examining this function and weighing the decrease in loss against the increased cost of processing, one would choose the number of channels to use for processing.

But, the calculations required for the above ideal procedure are so formidable as to make them impractical to carry out. The probabilities, p_{ij}, as heretofore defined, can be calculated only by an s-dimensional numerical integration or a Monte Carlo technique, when $k > 2$ and a normal maximum likelihood decision rule is used. If $s \geq 6$, the numerical integration is impractical even on the largest computers, and the Monte Carlo estimates are so imprecise and time-consuming as to be worthless for discerning small differences between subsets. Therefore, to simplify the task, we have made a number of approximations and assumptions in our procedures.

3.3. APPROXIMATIONS USED

First, each probability of misclassification, p_{ij}, is approximated by the corresponding pairwise p_{ij}, namely the p_{ij} that would apply if i and j were the only materials present. Figures 1 and 2 illustrate, for a one-dimensional problem, how this leads to overestimates of errors when other materials and decision levels are present. The overestimation is greater when distributions B and C lie on the same side of distribution A, as illustrated in Fig. 2. To simplify calculations, Type I and Type II errors* are averaged to obtain a single value for each pair of materials. The theoretical tendency of this approximation to overestimate errors has not been found of serious consequence in data sets processed to date, although resources have not been available for complete analyses. A few Monte Carlo checks of this approximation gave satisfactory agreements. A pairwise p_{ij} for $s = 12$ can be calculated by a quadratic method in about 3.5 seconds on our CDC-1604 digital computer. A general expression for the amount of overestimation can be obtained as follows

$$\text{True } p_{ij} = P_{ij} = P[f_i(X) = \max_k fk(X) \mid X \in \pi_j]$$
$$\text{Pairwise } p_{ij} = P^*_{ij} = P[f_i(X) > f_j(X) \mid X \in \pi_j]$$
$$\text{Difference} = P^*_{ij} - P_{ij} = P[f_k(X) > f_i(X) > f_j(X) \mid X \in \pi_j] \text{ for some } k \neq i, j.$$

However, the evaluation of these equations is not practical for multichannel data.

Second, l_{ij} is assumed equal to l_{ji}, and these cost factors are so normalized that

$$\sum_{j=1}^{K} \sum_{i=1}^{K} w_j l_{ij} = 1$$

The average expected loss is, therefore, a weighted average of p_{ij}'s and can be considered an average probability of misclassification. Thus, as a performance measure, the average expected loss has an intuitive meaning that provides a basis for choosing the subset size, a choice

*A Type I error is a failure to correctly classify a point from distribution A, while a Type II error is a false classification of a point from another distribution as being from class A.

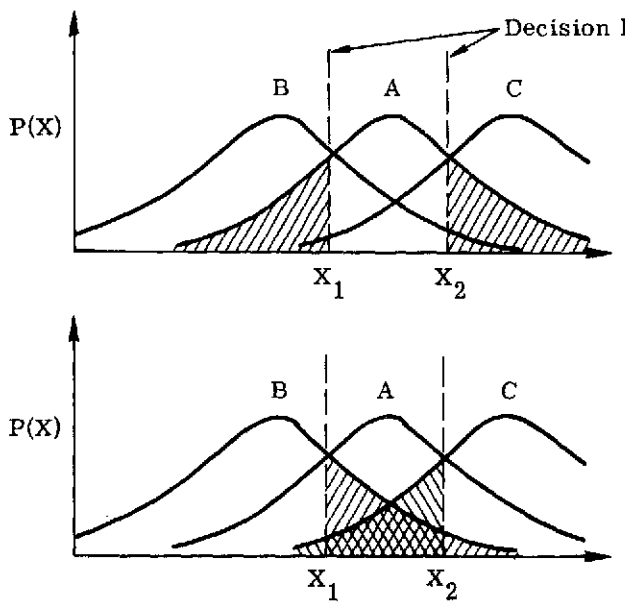

(a) Type I Errors:

True: $P_A(X < X_1) + P_A(X_2 < X)$

Pairwise: $P_A(X < X_1) + P_A(X_2 < X)$
(Exact)

(b) Type II Errors:

True: $P_B(X_1 < X < X_2) + P_C(X_1 < X < X_2)$

Pairwise: $P_B(X_1 < X < X_2) + P_B(X_2 < X)$
$+ P_C(X < X_1) + P_C(X_1 < X < X_2)$
(Overestimate)

FIGURE 1. ILLUSTRATION OF ERRORS FOR MATERIAL CLASS A, DISSIMILAR COMPETITORS

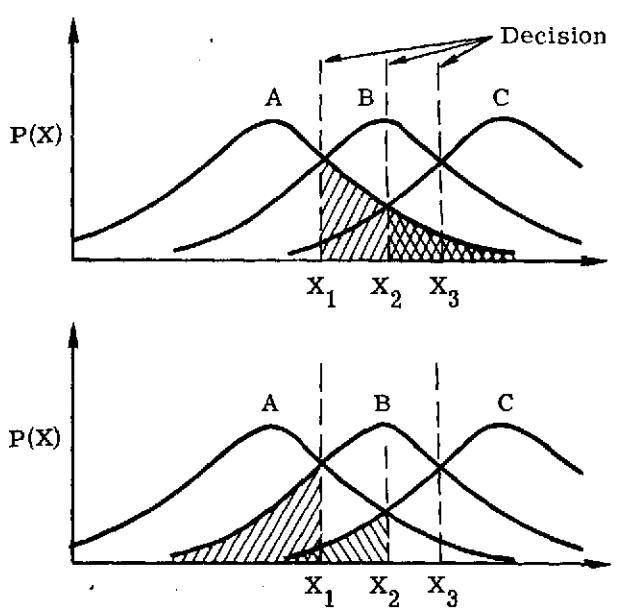

(a) Type I Errors:

True: $P_A(X_1 < X)$

Pairwise: $P_A(X_1 < X) + P_A(X_2 < X)$
(Overestimate)

(b) Type II Errors:

True: $P_B(X < X_1) + P_C(X < X_1)$

Pairwise: $P_B(X < X_1) + P_C(X < X_1)$
$+ P_C(X_1 < X < X_2)$
(Overestimate)

FIGURE 2. ILLUSTRATION OF ERRORS FOR MATERIAL CLASS A, SIMILAR COMPETITORS
(PAIRWISE ERRORS CROSS-HATCHED)

that requires a weighing of decision rule performance against processing cost. (Otherwise, this choice is made by an individual based on his experience and judgment.) We usually run the program with equal weights, w_j, but there may very well be some good reason for making the l_{ij}'s different. Suppose, for example, the signatures are barley, two kinds of wheat, and oats, and you want to be able to recognize the different crops but care nothing about discriminating between the two kinds of wheat. Equal l_{ij}'s would give the wheat-wheat p_{ij} equal weight with the other p_{ij}'s. Moreover, the wheat-wheat p_{ij} would probably be by far the largest, so the channels would be selected mostly on the basis of how well they distinguished between the two kinds of wheat. This unwanted result is avoided by making the wheat-wheat l_{ij} equal to zero. Or suppose one is mapping bodies of water and has signatures for shallow water, deep water, forest, crops, swamp, and bare soil. If the only errors that matter are those between a water and a land signature, these are the only pairs for which l_{ij} should be non-zero.

A third approximation is to choose the subset by a stepwise procedure, that is, by first choosing the best channel, next the channel which is best along with the one already chosen, then the channel which is best along with the two previously chosen, and so on. We have not tried this approximation without the pairwise approximation. In choosing a subset of size 5 from 10 channels, the time required by the stepwise approximation is reduced by a factor of 8. This approximation was tested on seven pairs of 10-channel signatures which were close together, had produced a confusing recognition map, and which, therefore, are believed to represent a demanding test of the approximation. All subsets of size 3 (and later of size 5) were ranked according to probability of misclassification. The stepwise procedure found the best subset for the subsets of size 3 of all pairs and for all but one pair of the subsets of size 5. In the one exception, the procedure picked the second of two subsets that were nearly tied for first place. It appears, therefore, that the stepwise procedure is a very good one.

The computer program that we have used during the past few years for channel selection, called STEPER2, incorporates the above three approximations; it requires a computing time of one hour on the CDC-1604 for rank ordering ten channels for a set of nine signatures.

Recently, we have studied ways of speeding up the calculations and have developed a fourth approximation which is to assume a linear approximation to the quadratic decision rule, thereby making a much simpler calculation of the probability of misclassification. Details of this approximation are presented in the appendix.

3.4. RESULTS

The new linear approximation was used to complete the hour-long job described above in 70 seconds, a 50-fold saving in time. Table 1 shows how results for the two methods compare. The probabilities computed by the two are comparable, and channel orderings are the same

except that the linear method, STEPLIN, interchanged the last two pairs of channels as compared to the order produced by the quadratic method, STEPER2. The use of channel 2 rather than channel 8 in a subset of seven channels would increase the average probability of misclassification by only 0.0001, according to the STEPER2 calculations. Similarly, the interchange of the last two ranked channels would increase the average by 0.00003 for a subset of nine channels. Although we did not repeat this comparison with different data sets, we did find close agreement when we later used several data sets to compare the linear and quadratic decision rules [6].

The seven close pairs of signatures referred to earlier were used to test the performance of three forms of the linear approximation (see appendix). All subsets of size 3 (and later all of size 5) were ranked by the quadratic and the three linear criteria, and the quadratic p.m. (probability of misclassification) for each subset was retained as a measure of performance. By this measure, the performance of all three linear methods was virtually identical and nearly as good as that of the quadratic method.

Table 2 gives, for each of the pairs of signatures: (a) the rank of the subset chosen by the fastest linear method, (b) the difference between the quadratic p.m. of that subset and the p.m. of the best subset, (c) the p.m. of the best subset, and (d) the difference between the p.m. of the worst subset and the p.m. of the best subset. The table shows that the linear method picked the best subset in 9 cases out of 14, did no worse than third for all but 2 of the cases, and, in the worst case, chose a subset with a p.m. only negligibly greater than the best p.m. The fourth column of the table shows how badly a poorly chosen channel selection method might perform. When one considers that time spent in a lengthy calculation of optimal channels would be better spent in adding more channels to the recognition process, the linear approximation in channel selection appears useful.

TABLE 1. COMPARISON OF CHANNEL SELECTION METHODS FOR NINE SIGNATURES

Quadratic Channel Selection (STEPER2)

Order of Channels	4	10	1	9	7	5	8	2	3	6
Average Probability of Misclassification	.119	.054	.031	.025	.023	.021	.019	.018	.017	.016

Linear Channel Selection (STEPLIN)

Order of Channels	4	10	1	9	7	5	2	6	6	3
Average Probability of Misclassification	.122	.059	.034	.028	.025	.024	.023	.021	.021	.020

TABLE 2. PERFORMANCE OF LINEAR CHANNEL SELECTION FOR SEVEN PAIRS OF SIGNATURES

Subset Size 3 (120 Subsets)

Rank of Subset Chosen	Linear p.m. - Best p.m.	Best p.m.	Worst p.m. - Best p.m.
4	.009	.110	.32
1	0	.081	.27
1	0	.110	.13
1	0	.023	.08
1	0	.006	.13
1	0	.010	.25
1	0	.035	.29

Subset Size 5 (252 Subsets)

Rank of Subset Chosen	Linear p.m. - Best p.m.	Best p.m.	Worst p.m. - Best p.m.
9	.006	.090	.24
1	0	.072	.23
2	.000	.082	.10
1	0	.013	.04
1	0	.004	.07
3	.000	.006	.04
2	.000	.022	.15

4

THERMAL CHARACTERISTICS AND RECOGNITION PROCESSING

Recognition processing with visible and near-infrared data channels depends only on reflectance characteristics of the surface materials, instantaneous irradiation, and viewing geometry. These quantities determine the observed radiance in conjunction with atmospheric effects. The physics of thermal data are different because current temperature depends on past temperature and local meteorology as well as on thermal characteristics of the materials. These differences influence recognition processing of data collected simultaneously in reflective and thermal channels in several ways as discussed below.

The spectral emittances of most natural materials are high (≥ 0.9) and without significant spectral structure in the thermal infrared region (4 to 30 μm) of the spectrum. Thus, differences in observed radiances are primarily caused by differences in temperatures. One exception is in geology where the spectral emittances of various rock types exhibit bands of low emittance in the 8- to 12-μm region, caused by the restrahlen effect [30]. However, because geologic applications and appropriate processing techniques (such as thermal ratio methods) are treated in another report under this contract [7], the subject is not discussed further here.

The major influence of differences between thermal and reflective data is expected to be in the area we call "signature extension," that is, in transformations to make spectral signatures applicable to regions removed in time and/or space from the regions used for training (i.e., for signature extraction). In reflective data, two types of effects have been identified—(a) across-track, or scan-angle, effects and (b) along-track,or time-dependent, effects. Scan angle effects occur primarily because of different path lengths, view geometries, and surface bidirectional reflectance characteristics. Along-track effects occur because of changing sun position, changing atmospheric conditions, and changing surface conditions. Most effort to date has been expended on studies of scan angle effects.

Our experience with scan angle effects shows that generally they are wavelength-dependent and apt to be less pronounced in thermal data than in reflective data [8a]. The 1971 Corn Blight Watch data provides a case in point. In WRL processing of Corn Blight Watch data on the SPARC analog computer, it was decided to use only subsets consisting of six of the twelve available channels to permit more classes of materials to be used.* Purdue University personnel were to select and provide WRL with one such subset for each group of data. Subsequently, upon examination at WRL, it was found that in six of the ten subsets furnished, the thermal channel was included. Overall, of the 12 channels available, the thermal channel was selected most frequently as a member of channel subsets used for processing Corn Blight Watch data [8b].

*The product, (number of channels) × (number of classes), has a fixed maximum value on the SPARC system.

The other aspect of signature extension is the treatment of those along-track and set-to-set variations that are systematic in nature. As noted earlier, reflective signatures depend on the instantaneous condition of the surface and the viewing and illumination geometries. Thermal signatures depend on the recent history of surface heat balances, and the length of history that is important depends on the type of surface. Leaves of growing plants respond quickly to changes in radiant input, while more massive materials such as rocks and soil respond more slowly. These differences can be important for recognition when cloud shadows are moving across a scene being mapped. The remainder of this section examines these differences more closely.

One investigator [9] has shown that the 50-percent temperature time constants of leaves subjected to changing thermal inputs in laboratory experiments are on the order of ≈45 seconds. Furthermore, Gates [10] and others have shown that leaf temperatures are coupled to prevailing air temperatures when there is any appreciable amount of wind. However, the prediction of leaf temperatures is by no means simple because they depend on the availability of moisture in the leaves, the relative humidity of surrounding air, the wind, and the radiation input. Leaf temperatures may be either higher or lower than air temperature, depending on the specific combination of conditions present. Storage of heat energy in leaves is minimal, so their temperatures would rapidly recover from being in cloud shadows and their relevant temperature histories are short.

Bare soil, on the other hand, has a longer relevant temperature history because of its greater thermal inertia and capacity. Calculations were made with the temperature prediction model which had been developed earlier at WRL to assess the effect of a passing cloud shadow on the temperature of bare soil [11].

Figure 3 presents computations of soil temperature for two conditions: (1) a typical clear day with no clouds to reduce the solar input radiation and (2) the same day except that a cloud shadow obscured the surface from direct solar radiation for one hour (from 11 A.M. to 12 noon). Immediately after the cloud shadow was removed, the temperature was found to be $10^{\circ}F$ ($4.4^{\circ}C$) cooler than when the shadow began, and $21^{\circ}F$ ($9.2^{\circ}C$) cooler than unshadowed soil. It took about 8 minutes for the temperature to attain the 11 A.M. value and, although the temperature continued to increase until 4:30 in the afternoon, it never matched that of the unshadowed soil. Thus, one can see that shadows occurring several hours before data collection can influence the temperatures of scene materials viewed by a scanner. This complicates along-track and set-to-set signature extension problems in thermal channels. Short-term shadow effects also are shown.

The material chosen for the calculations was a Dakota Sandy Loam with a dry density of 110 lb/ft^3 (1.762 gm/cm^3). Six layers with a total thickness of 63 cm were assumed; individual thicknesses, from the top, were 1, 2, 4, 8, 16, and 32 cm. Soil moisture was 11% by weight, or 1/3 of complete saturation. The peak solar radiation input was equivalent to one passed through

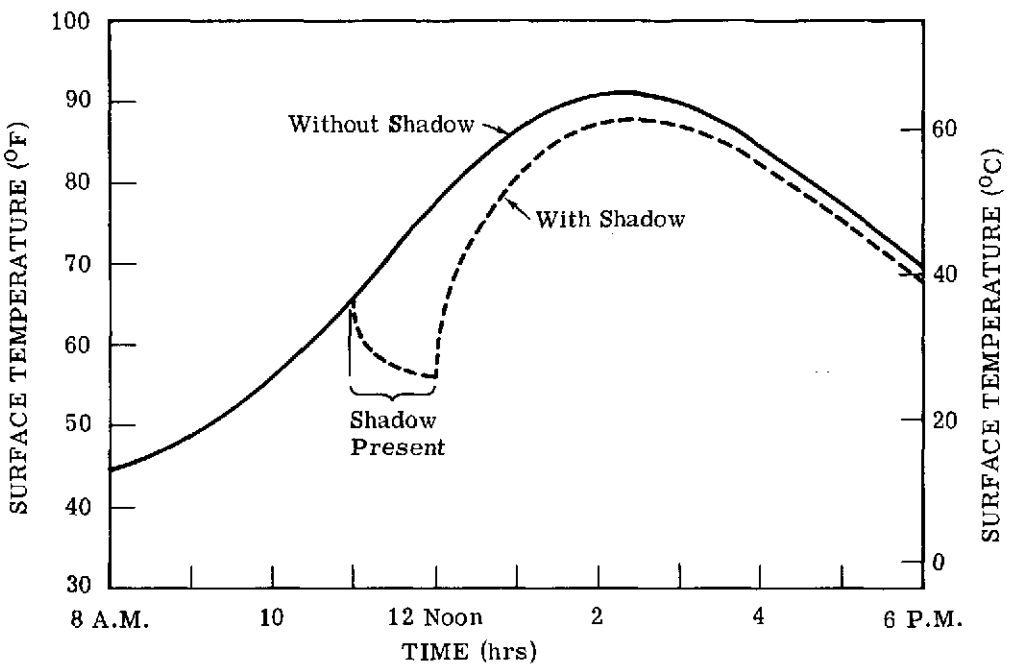

(a) Long-Term Influence of One-Hour Shadow

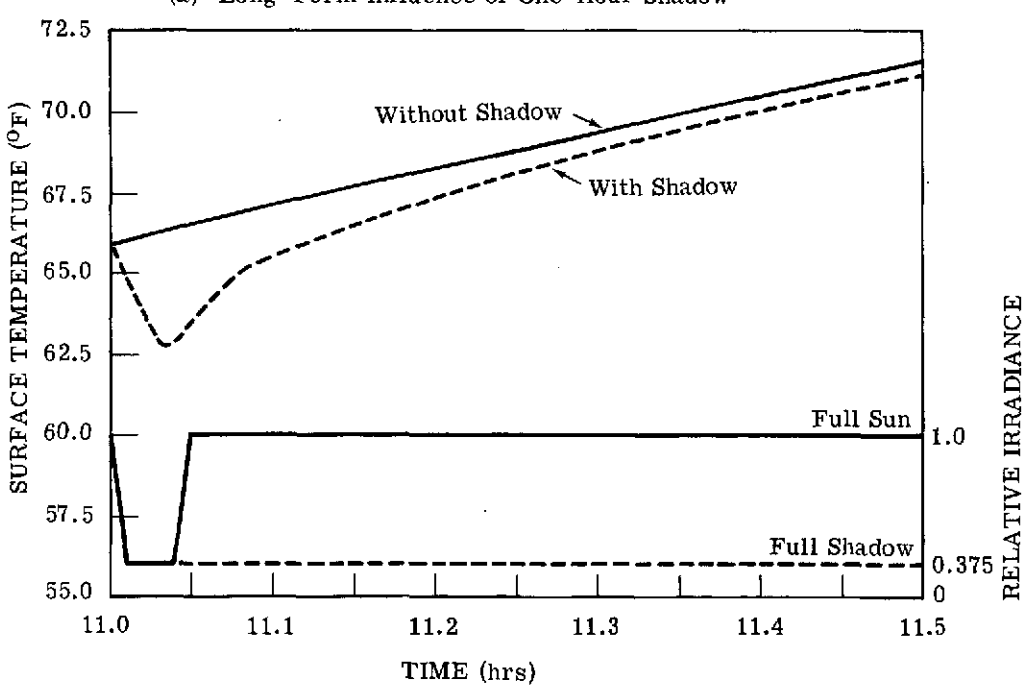

(b) Short-Term Influence of Three-Minute Shadow

FIGURE 3. CALCULATED INFLUENCE OF CLOUD SHADOWS ON SOIL TEMPERATURE

1.5 atmospheres (i.e., the air mass m = 1/sec θ = 1.5, where θ = solar zenith angle). For the duration of the shadow, 1/8-th of the full value was used. Wind velocity was constant at 6 mph, while the relative humidity was 80%.

5
RADIATION-BALANCE MAPPING

The ability of multispectral scanners to map radiances emanating from the Earth's surface in various spectral bands has been demonstrated many times, and multispectral pattern recognition techniques have been used to identify the classes of surface materials present in scenes. Heretofore, little attention has been directed toward use of attributes derived from the multispectral signals for interpretation of scene conditions. Surface exitance* and surface radiation balance are derived attributes considered in this report. Radiation is the principal form in which the sun transmits energy to Earth for the sustenance of life. While ground instrumentation can provide point measurements of incident radiation and radiation balance, only airborne and spaceborne multispectral scanners can provide synoptic and quantitative measurements over large areas. Such measurements are applicable to many disciplines —agriculture, forestry, hydrology, meteorology, physical geography, and urban climatology. This universality results in large part from the linkage between radiation balances and water balances of terrestrial ecosystems, and the energy budget relationships implicit therein.

Succeeding text in this section considers: the nature of radiation balances; important factors in measuring surface radiation with multispectral scanners; techniques for estimating and mapping surface exitance and incidance and radiation balance; the interrelationships between radiation balance, energy budget, and evapotranspiration; illustrative applications of the techniques to agricultural and urban scenes; and related development of special-purpose computer programs.

5.1. RADIATION BALANCE

As a planet, the Earth maintains a constant average annual temperature because the radiation output at the top of the atmosphere just equals, or balances with, incoming radiation when both are averaged globally for a year over all wavelengths [12]. This is not the case, in general, for any specific latitude or for any shorter period such as a season, month, day, or minute. Furthermore, incoming and outgoing radiation streams generally would not be expected to balance or equal each other at the interface between Earth's surface and the atmosphere. Net radiation (incoming minus outgoing) and its partitioning into components of energy budgets are of interest here, including radiation at both long and short wavelengths.

In radiation balance and energy budget studies [10, 11], it is conventional to discuss two broad wavelength categories of radiation. These categories comprise: (1) short-wavelength solar radiation from 0.3 to about 3 μm and (2) long-wavelength thermal radiation from about 3 to 30 μm. These divisions come about for at least two reasons. First, the direct contribution

*Exitance is the outgoing radiant flux density, e.g., W/m^2 leaving surface.

of solar radiation is insignificant in the long-wavelength interval compared to that from the atmosphere. Second, measurement instruments (e.g., pyronometers) incorporating glass domes are effective only in the short-wavelength interval.

The short-wavelength solar radiation that reaches the Earth's surface has both a direct component and an indirect or diffuse component. The direct component is reduced as it passes through the atmosphere because of transmission losses along the path. The diffuse component occurs because of scattering by aerosols and molecules in the atmosphere; clouds also can produce indirect radiation by reflection. The radiant flux density on a horizontal unit area is the incidance, E; it is measured in units of watts·m^{-2} which are gaining acceptance over another common unit, cal·cm^{-2}·min^{-1} sometimes called langleys·min^{-1}.

At the top of the atmosphere, the normal incidance of the sun is approximately 1396 W·m^{-2} or 2 ly·min^{-1}. The total (direct and diffuse) amount reaching a horizontal surface on the Earth is typically 700 to 900 W·m^{-2} at midday at mid-latitudes. A substantial amount of thermal radiation from the atmosphere also reaches the Earth's surface. It results from thermal emission by air molecules, aerosols, and any clouds present. On a typical summer day at mid-latitudes, the thermal incidance from the atmosphere might be 300 to 400 W·m^{-2}.

Radiation leaves the Earth's surface at short wavelengths by reflection and at long wavelengths primarily by thermal self-emission. Typical values are 140 and 420 W·m^{-2} respectively.

For an opaque, diffusely reflecting surface, we can write a simple equation for the net incoming radiant flux density (that is, for the balance of radiant flux on a surface of unit area):

$$E_{Net} = (1 - \rho)(E_S + E_s) + \epsilon E_T - M_T \qquad (4)$$

where

E_{Net} is the net radiant incidance
E_S is the direct solar incidance
E_s is the indirect, or diffuse, solar incidance
ρ is the diffuse hemispherical reflectance (sometimes called albedo) of the surface (values between 0.05 and 0.30 in the absence of snow [12, p. 21])
E_T is the thermal incidance
ϵ is the thermal absorptance (emissivity) of the surface (a value between 0.90 and 0.96 for most natural objects)
and M_T is the thermal exitance of the surface [i.e., self-emitted thermal radiation which depends on both the temperature, T_s, and the emissivity of the surface; $M_T(T_s) = \epsilon \sigma T_s^4$, where the Stefan-Boltzmann constant $\sigma = 5.67 \times 10^{-8}$ W·m^{-2} $^oK^{-4}$].

All quantities except ρ and ϵ, which are dimensionless, have units $W \cdot m^{-2}$ (or $ly \cdot min^{-1}$). Eq. (1) can be rewritten as follows:

$$E_{Net} = [E_S + E_s + \epsilon E_T] - [\rho(E_S + E_s) + M_T]$$

$$= [\text{Incoming radiant flux density}] - [\text{Outgoing radiant flux density}] \quad (5)$$

$$E_{Net} = E_{Total} - M_{Total} \quad (6)$$

Here, E_{Total} is the total incidance, while M_{Total} is the total exitance. When the surface is not a diffuse reflector and emitter, Eqs. (4) and (5) become more complex. For example, the reflected radiation from a non-diffuse surface depends on the spectral distribution of the incoming radiation, so the same reflectance term should not be applied, in general, to the direct and indirect components of solar radiation in Eqs. (4) and (5). This is considered in more detail below.

5.2. MEASUREMENT CONSIDERATIONS

Exitance, a measure of the radiation leaving a surface, is one of many attributes that can be derived from multispectral scanner measurements. However, airborne and spaceborne multispectral scanners cannot completely measure surface exitance; rather, they sample the radiation from the surface —spectrally, spatially, and temporally —through the atmosphere which attenuates the surface radiation and also adds extraneous radiation. The discussion which follows considers methods of making accurate estimates with a minimum of ground information. Other approaches are discussed in Section 5.6.

5.2.1. SENSOR CHARACTERISTICS

Spectral sampling is partly a result of atmospheric absorption. The self-emitted spectral radiance from a 300°K surface is maximum at about 10 μm, and remains significant over the spectral region from 4 to 30 μm. However, the atmosphere absorbs radiation extensively throughout much of this spectral region. Measurements made at those wavelengths for which the atmosphere is relatively transparent (i.e., in so-called "windows") can be used to estimate the total thermal radiance of the surface.

The near-infrared region of the spectrum also has atmospheric windows between several prominent absorption bands, and the visible region itself is in an atmospheric window region. Multispectral scanners are designed to synoptically sense and record radiation at one or more spectral intervals in these window regions [3].

Two spatial sampling characteristics of multispectral scanners are important. First, a scanner measures the surface radiance ($W \cdot m^{-1} \cdot ster^{-1}$) within a narrow solid angle, but exitance

($W \cdot m^{-2}$) is defined as radiance into a hemisphere. Second, the angular field of view and the limits of the scan angle when coupled to the sensor altitude, lead to definitions of scanner ground resolution element size and area of coverage, respectively. Current airborne multispectral scanners have angular resolution of 2 to 5 mrad. At altitudes of 0.3, 3, and 15 km, the widths of the ground resolution elements corresponding to 2 mrad at nadir are 0.6, 6, and 30 m, respectively. Ground resolution elements for multispectral scanners on the Earth Resources Technology Satellites (ERTS) and the SKYLAB Earth Resources Experiment Package (EREP) are or will be 80 m wide or larger; the width of the resolution element of the medium resolution radiometer on the Nimbus II meteorological satellite is 50 km at nadir. Thus, it can be seen that the portion of a scene observed in a single resolution element can vary considerably depending on the sensor characteristics and altitudes.

The maximum off-nadir scan angle limits the total width of data collected on a pass by a scanner and influences the amount of scan-angle dependence found in the data. For airborne scanners, the off-nadir scan coverage is typically $\pm 30^{\circ}$ to $\pm 45^{\circ}$, but for satellite scanners is only only a few degrees. For $\sim 30^{\circ}$, at altitudes of 0.3, 3, and 15 km, the swath widths would be 0.36, 3.6, and 18 km, respectively. Swath widths for the previously mentioned EREP, ERTS, and Nimbus II satellite scanners are 68 km, 185 km, and roughly 2000 km, respectively.

The linear dimension of coverage along the flight line is determined by the speed of the platform and the duration of data collection (which is limited at times by the data recording capability). Typical non-jet aircraft speeds are 200 to 600 km/hr. ERTS and EREP ground speeds are both roughly 7 km/sec (25,200 km/hr).

Because a remote sensor measures instantaneous radiation values, time-integrated effects, if needed, must be determined from multiple passes, continuous ground-based measurements, and/or model calculations.

5.2.2. ATMOSPHERIC CHARACTERISTICS

In meteorological satellite studies of radiation balance, the atmosphere is part of the system being measured. Estimation of actual surface radiation balances from satellite or aircraft data is more complex because the atmosphere becomes an intermediate and interfering medium. Airborne-measured radiance consists of two parts: (1) radiance of the surface after transmission losses through the atmosphere to the scanner and (2) extraneous path radiance produced by the atmosphere.

Atmospheric transmittance and path radiance vary spatially as well as spectrally. For both, the spatial dependence at short wavelengths is related to the direction of view relative to the nadir; for path radiance, this dependence also relates to the sun's position. Spectrally, the radia-

tion that reaches the surface is modified by the atmosphere. The near-infrared region of the spectrum has windows of high transmittance roughly from 3 to 4 μm, 2.0 to 2.4 μm, 1.5 to 1.8 μm, and 0.7 to 1.4 μm with lesser absorption bands in the 1.1 to 1.15 μm and 0.93 to 0.96 μm intervals. The visible spectrum, 0.4 to 0.7 μm, is in a window region which extends to approximately 0.3 μm in the ultraviolet; the amount of radiation absorption is low but scattering from atmospheric particles becomes more severe as the wavelength decreases. Consequently, spatial contrasts and the proportions of useful radiation are low at blue and ultraviolet wavelengths.

Radiative transfer models can be used to estimate these atmospheric effects for both solar [14] and thermal [15] radiation to improve the accuracy of exitance and radiation balance estimates based on remotely sensed data.

5.3. ESTIMATION AND MAPPING OF EXITANCE

To estimate total surface exitance from multispectral scanner data, one should take into account the sensor's spectral sampling characteristics, spatial reflectance and emittance characteristics of the observed surface, and atmospheric effects. Equations (4) and (5) assume that observed surfaces have Lambertian (diffuse) reflectance and emittance characteristics, i.e., that the spatial distribution of the outgoing radiance obeys a cosine law and, for reflection, is independent of the spatial distribution of incoming radiation. Natural surfaces depart from these idealized properties —introducing errors if this departure is not properly incorporated into the estimation procedure. Both the angles of view and illumination [16] and the overall spatial distribution of exitance are important.

For thermal radiation, the spectral shape of the emitted radiation from vegetation is essentially that of a blackbody radiator [30]. If the sensor response function is known and the atmospheric effects in the spectral window are calculated, all the necessary information is available for estimating the total thermal radiance of the surface. The remaining task is one of establishing the spatial emission characteristics of the surface in order to convert radiance ($W \cdot m^{-2} \cdot ster^{-1}$) to exitance ($W \cdot m^{-2}$). For a Lambertian surface, exitance is π times the radiance. Non-Lambertian thermal emission characteristics have not been investigated widely; however, in at least one study, empirical corrections have been extracted and applied to meteorological satellite data [17].

For short-wavelength radiation, the spectral reflectance function differs with material so one cannot assume a standard spectral shape. However, if wavelength intervals are chosen to match the atmospheric windows, most of the exitance is measured, owing to the fact that atmospheric absorption reduces the incidance on the surface at the non-window wavelengths. Summation of corrected radiance values from several channels then represents an integration over

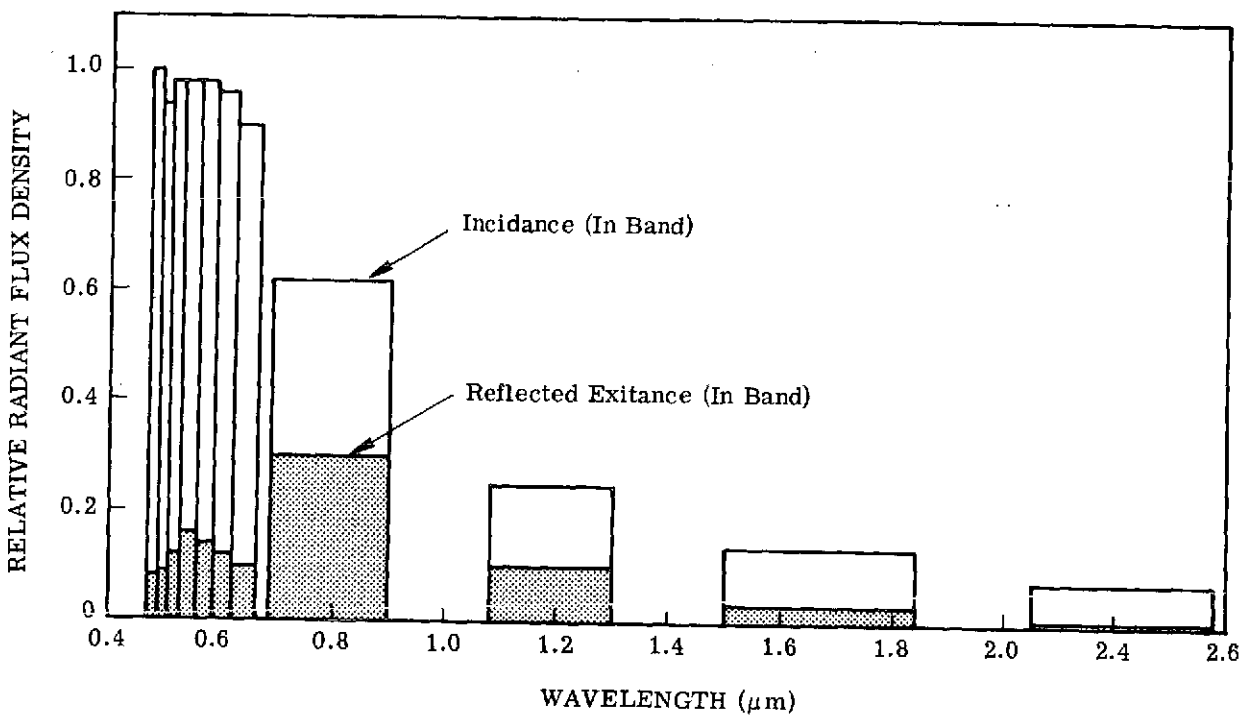

FIGURE 4. ESTIMATED DISTRIBUTIONS OF INCIDENT AND REFLECTED RADIATION, FOR AVERAGE GREEN VEGETATION SURFACE, IN CHANNELS OF MICHIGAN MULTISPECTRAL SCANNER

the spectrum of interest; weighted summation can be used to adjust for spectral sampling. Figure 4 presents a reflective exitance spectrum for green vegetation as might be obtained from the Michigan M-7 multispectral scanner. This spectrum was obtained from the peak-normalized product of the solar irradiance curve, an average reflectance of green vegetation, and the spectral response functions of the M-7 scanner. Note the high proportion of exitance in the 0.69-0.90 μm band.

The spatial conversion from narrow-angle radiance to hemispherical exitance is complicated by the fact that short-wavelength exitance depends on illumination geometry in addition to view angle. In other words, the bidirectional reflectance properties of the surface are involved so the Lambertian assumption is not entirely adequate. To correct exitance calculations for spatial effects, recently developed mathematical models of the bidirectional reflectance of vegetation canopies can be used [18].

For scenes of interest, the short- and long-wavelength exitances can be, and have been, computed and mapped separately [19]. Summation of the two components provides the desired estimate of the total exitance which can also be mapped [4, 20]. Exitance maps permit scene differences to be examined on a gross level for major cover types or on a detailed level within a cover type.

5.4. INCIDANCE ESTIMATION AND RADIATION BALANCE MAPPING

An estimate of total incidance is required in order to calculate a radiation balance from multispectral scanner data. There are various ways of obtaining this estimate. First, ground instrumentation may be located strategically along the flight path. Second, weather station data (including meteorological soundings) may be used as inputs to radiative transfer models for computing both the solar and thermal inputs. Third, auxiliary sensors on airborne platforms can provide additional information for estimating incidance and atmospheric effects. For example, a sun/sky sensor coupled with the Michigan scanner provides a measure of solar incidance at the sensor altitude. If obtained at several different altitudes, the sun/sky sensor data can help characterize the atmospheric state. Also, up-looking and down-looking pyranometers mounted on aircraft have been used to measure spectrally integrated solar radiation fluxes on the Michigan aircraft and elsewhere [21]; similarly, thermal pyrgeometers can be used to measure thermal fluxes [12, Chap. 6].

Exitance determined from multispectral scanner data (as discussed in Section 5.3) can be subtracted from estimates of incidance from model calculations and/or auxiliary sensor measurements to obtain radiation balance estimates [19, 20]—i.e., estimates of the net radiant flux density input to the surface systems observed. Maps of net radiation can then be produced [4, 20].

The following hypothetical example based on available theoretical and measured values illustrates the relative magnitudes of the spectrally integrated components of a radiation balance at mid-day at mid-latitudes:

Quantity	Incidance ($W \cdot m^{-2}$)	Quantity	Exitance ($W \cdot m^{-2}$)
Direct Solar Radiation	700	Reflected Solar Radiation (770×0.18)	140
Diffuse Solar Radiation	70	Emitted Thermal Radiation	420
Atmospheric Radiation Thermal (368×0.95)	350		
E_{Total}	1120	M_{Total}	560

$$E_{Net} = E_{Total} - M_{Total} = 1120 - 560 = 560 \ W \cdot m^{-2}$$

5.5. RELATIONSHIPS BETWEEN RADIATION BALANCE, ENERGY BUDGET, AND EVAPOTRANSPIRATION [22]

Every object, area, and volume maintains, on a long-term average, a balance between the energy it receives and that which it gives up. Of the several physical processes by which energy is exchanged, radiation has the controlling influence on the energy budgets of surface features. In fact, the usual energy balance equation equates the net energy received in the form of radiation (over all wavelengths) to the sum of the various sinks into which this energy is dissipated or distributed.

Before we continue, a problem in semantics must be resolved. Notations and terminology used up to this point for the description of radiation quantities are as preferred by the remote sensing community and the Optical Society of America. Different notation is used in the meteorological and agricultural literature to describe radiation, evaporation, and heat fluxes for the energy balance relationship; some of the symbols are the same as used in this report for radiation quantities. Since no single unified notation scheme appears to exist for energy balance descriptions, the one presented below is arbitrarily assigned and other common symbols noted as appropriate.

The vertical energy balance relationship for a surface in terms of flux densities (as may be measured in units of $W \cdot m^{-2}$) is an equating of the net incoming radiation (Eq. 6) with the non-radiative energy sinks:

$$E_{Net} = F_E + F_H + F_G + F_P + F_M \tag{7}$$

where E_{Net} = net radiant incidance, also called net radiation and denoted by R_n or R,

F_E = latent heat flux density (i.e., heat loss to evapotranspiration), also denoted by E, ET, L, or LE,

F_H = sensible heat flux density (i.e., heat loss to the air by convection), also denoted by H or A,

F_G = soil heat flux density (i.e., heat conducted to the soil), also denoted by G or S,

E_P = net rate of energy conversion by the community (e.g., photosynthesis minus respiration for plants,

F_M = miscellaneous heat flux densities (e.g., losses by advection).

Upon integrating over a selected time interval and multiplying by the given area, one obtains the corresponding energy components* into which the net absorbed radiant energy is partitioned.

$$Q_{Net} = Q_E + Q_H + Q_G + Q_P + Q_M \tag{8}$$

where Q_{Net} = net incoming radiant energy over all wavelengths
Q_E = latent heat energy loss to evapotranspiration
Q_H = net turbulent sensible heat energy loss to the air
Q_G = energy loss by conduction to the soil
Q_P = net energy conversion
Q_M = miscellaneous heat energy sinks

For many situations, the last three terms can be neglected and, to a first approximation,

$$Q_{Net} = Q_E + Q_H \tag{9}$$

especially when averaged over a period of one or more days.

Figure 5, reproduced from Fig. 33 of Ref. [12], illustrates some of the extremes that can be encountered in diurnal variations of the energy budget components on a flux-density basis. These data are for an irrigated alfalfa-brome hayfield at Hancock, Wisconsin (Tanner and Pelton); a small stand of irrigated Sudan grass at Tempe, Arizona (Van Bavel and Fritchen); and a barren dry lake near El Mirage, California (Vehrencamp). The hay and Sudan grass were 15 and 100 cm high, respectively, and were watered well. Skies were clear, winds light to moderate, and air temperatures as indicated on the figure.

In Wisconsin, the loss rate by evapotranspiration was the greatest of the components and dissipated approximately half of the net radiant power input. Note that non-radiative losses are plotted positive, while gains are negative. In Arizona, where the evapotranspiration loss rate actually exceeded the available radiation rate, the additional energy input to the surface was obtained by advection from the hot, dry air as it passed over the small watered site. In California, there was very little water available and, consequently, minimal evaporative heat loss.

5.5.1. ENERGY BALANCE METHOD FOR DETERMINING EVAPOTRANSPIRATION**

Consider the following rearrangement of Eq. (7), the balance equation for energy flux density:

$$F_E = E_{Net} - F_H - F_G - F_P - F_M \tag{10}$$

*Common units for energy are joules; however, many investigators do not multiply by area, preferring instead to work in energy density units such as joules/m^2.

**For a more comprehensive treatment, see Refs. [12, 20, 23, 24].

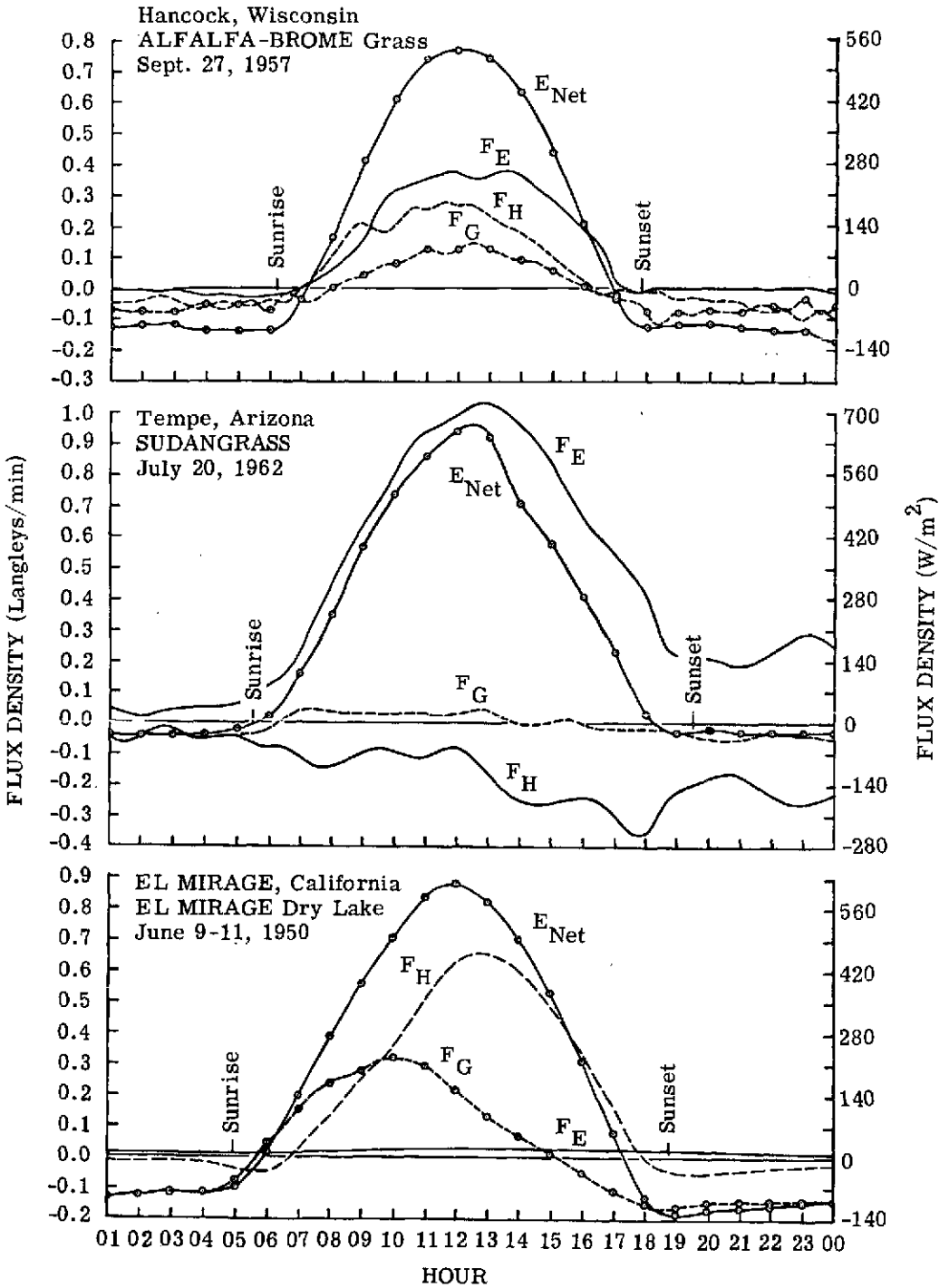

FIGURE 5. AVERAGE DIURNAL VARIATION OF SURFACE ENERGY BALANCE COMPONENTS. Over grass at Hancock, Wisconsin, and Tempe, Arizona, and over bare soil at El Mirage, California. (After Fig. 33 of Ref. 12.)

The rate of heat loss to evapotranspiration, F_E, can be determined if all the quantities on the right-hand side of the equation are measured or estimated. F_M and F_P are usually negligible, but if not, can be estimated or measured. F_G and E_{Net} are relatively easy to measure in the field. This leaves the sensible heat term, F_H, as the only other unknown quantity. It too can be measured by either the aerodynamic profile method or the eddy correlation principle; however, the instrumentation is not as simple as for the other measurements. In the absence of measurements of F_H, the Bowen ratio can be estimated from general knowledge of percent ground cover, magnitude of E_{Net}, relative humidity, and supply of water in the soil. The Bowen ratio is $\beta = F_H/F_E$, or the ratio of sensible to latent heat flux densities.

Remote sensors can serve as a means for extrapolating ground measurements from a few points to an entire scene, provided clear sky conditions prevail. They will detect differences of two types—different albedos and different temperatures. For a given class of community with the same albedo, a temperature difference could indicate a moisture-stress condition [23]. According to Ref. [20], the opinion of authorities, in 1965, was swinging strongly toward the view that the evaporation rate does decrease as the soil moisture potential decreases even though other conditions remain the same.

A more sophisticated use of remote sensors would be to use their calibration capability to make quantitative estimates of the net radiation of scene communities without reference to the ground measurements.

5.5.2. OTHER METHODS FOR DETERMINING EVAPOTRANSPIRATION*

There are several other methods for determining evapotranspiration rates: (1) water balance method, (2) the eddy correlation method, (3) the aerodynamic or profile method, and (4) the combination method. Except for the last method named, remote sensing techniques cannot provide useful inputs.

Water balance methods include catchment hydrology wherein precipitation, interception, runnoff, and changes in water storage are measured. Another such method involves the measurement of soil moisture depletion. The most accurate water balance method is lysimetry, which requires that the experimenter have complete knowledge of all the water components.

Eddy correlation methods make use of the fact that the instantaneous mass of water vapor flux can be computed from the vertical velocity of wind and the concentration of water vapor. Equipment complexity and sensor limitations have restricted widespread use [24].

*For more details on these methods, see Refs. [12 and 22-27].

The aerodynamic or profile method employs measurements of the differences in vapor pressure, temperature, and horizontal wind velocity at two or more heights above the canopy.

The combination method represents a combination of the energy balance method and the aerodynamic method. Originally proposed by Penman [28], it involves a quantity called "potential evapotranspiration." Potential evapotranspiration has been used to define the water loss from a land surface that is completely covered by vegetation, has adequate moisture at all times, and is large enough for oasis effects (advection) to be negligible [23, 26, 28]. This potential evapotranspiration (or water need) is limited solely by the energy available in the form of absorbed radiation and the capacity of the air to receive and hold more water vapor. According to Thornthwaite (1965) [23], the type of vegetation cover does not make a great deal of difference except through its reflectance which determines the fraction of incident radiation absorbed.

Actual evapotranspiration is frequently less than potential evapotranspiration because it depends on water supply and other field conditions. As the water supply in soil progressively decreases below field capacity, less evapotranspiration takes place. The fraction of absorbed energy that is no longer used for furnishing the latent heat of evaporation must be dissipated by heating the air, by conduction in the soil, and/or by increased thermal emission resulting from higher temperatures. Furthermore, actual field conditions frequently depart from the idealized "potential" conditions, particularly near boundaries where advection can become important. Plants under moisture stress would be expected to have radiation balances that differ from similar plants with adequate water supplies.

5.6. APPLICATIONS IN AGRICULTURE AND URBAN STUDIES

In estimating and using exitance and radiation balances,four levels of increasing sophistication can be identified. First is the mapping, on a relative basis, of apparent* radiation quantities (e.g., exitance or radiation balance) over various portions of the scene. The second entails mapping absolute values of the apparent radiation quantities. The third is with atmospheric compensation provided. Map outputs like those mentioned above can be interpreted manually by trained image interpreters. On the fourth level is the use of the data for quantitative analysis and interpretation of physical and/or biological phenomena in the observed materials.

Maps of the estimated quantities on an apparent or relative basis provide an investigator with aids —in addition to the standard imagery and recognition maps —for the discovery and investigation of differences in scene materials. Upgrading the data base by correction for atmospheric effects would give an investigator a map based upon better estimates of the true differ-

*That is, data mapped without compensation for atmospheric effects.

ences observed. Such an upgrading can be accomplished by calibrating the estimation constants with a few ground-based measurements made within the scene at the time of the overflight or, as discussed above, by using sensor data calibration, auxiliary data, and/or theoretical calculations of atmospheric effects.

A quantitative analysis and interpretation can be made of exitance and radiation balance differences, both between classes of materials (inter-class analysis) and within particular classes (intra-class analysis). The aim of such analyses is to relate the observed differences in the estimated quantities to physical and/or biological differences in the observed materials — first on a relatively manual basis, but ultimately as an automated part of the process of extracting information from multispectral scanner data through computer processing. Although moisture stress in vegetation has been mainly discussed herein, differences due to stress of all kinds are potentially detectable. Other stresses include those of disease, insects, salt, and/or nutrient unbalance.

A map of apparent exitance can be used to examine differences between various surface materials in a scene on both gross and detailed levels. For example, Fig. 6 is a digital map of an agricultural scene showing the total apparent exitance as determined from multispectral scanner data in a manner discussed in detail later in this section. High exitances are presented in light tones. On the gross level, one can identify the small dark spots in the lower left hand corner; these are the individual trees in a young orchard. The dark semicircular area above them is wet bare soil, and dry bare soil lies to the right; less radiation leaves the wet soil because it is darker (thereby reflecting less radiation) and cooler because evaporation uses much of the absorbed energy. Two corn fields are at the right of the map; the lower one appears slightly darker because it was more mature, reflected less near-IR radiation and, probably due to greater evapotranspiration, was cooler than the upper field.

On a detailed level, an apparent exitance map permits one to assess the uniformity of the energy dissipation pattern within individual fields. Some irregularities in the lower corn field are due to plant differences caused by a disease, namely corn blight. On the other hand, the upper field exhibits a broad pattern caused by the particular scanning geometry employed; this artifact should be discounted. Differences in moisture availability or drainage patterns should be readily seen when present. Furthermore, field edge effects due to prevailing winds should be discernible. One can also use the exitance map to assess the extent to which any sites observed by ground instrumentation are representative of the fields in which they are located.

Investigators have begun to study the radiation environment of urban areas as an important aspect of human living conditions. An example total exitance map of a golf course is presented in Fig. 7b. Lambertian surfaces were assumed and the gray scale used for the map presents the greater exitances in the lighter tones. Exitance differences for various grasses on the greens, fairways, and rough are evident. A black-and-white infrared (0.7-0.9 μm) photograph

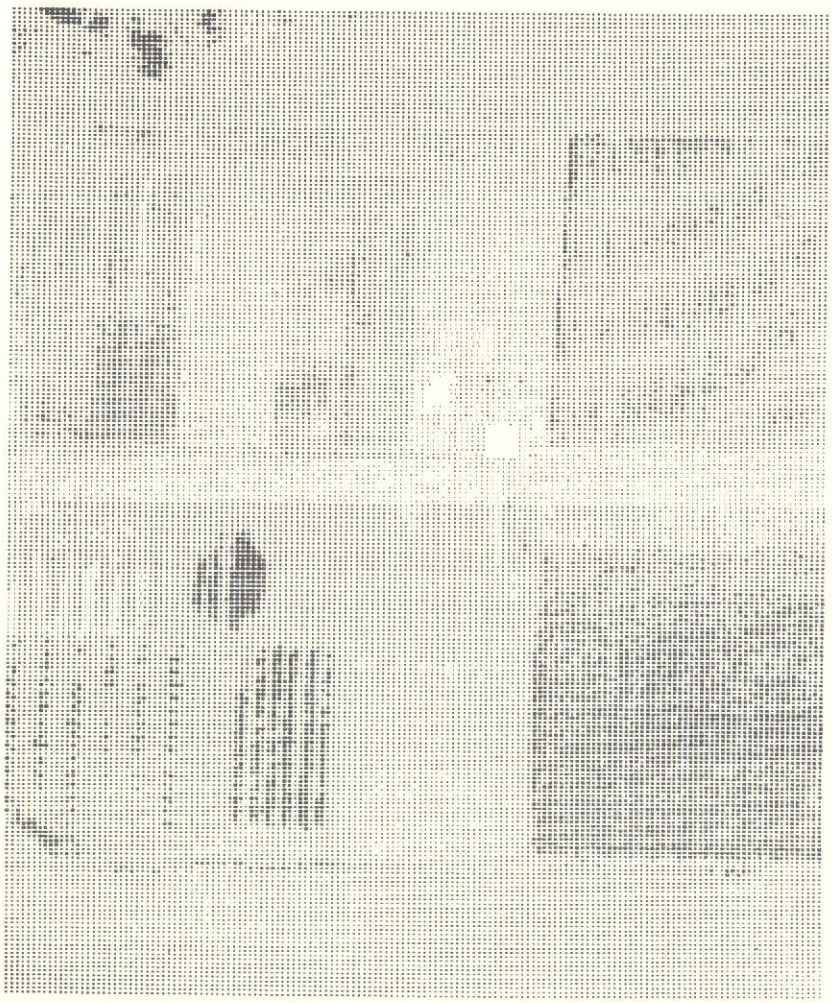

FIGURE 6. EXAMPLE EXITANCE MAP, AGRICULTURAL SITE
(6 AUG. 1971, ALT = 1000 FT, 11:16 EST, MSU).
Light tones, represent high values of total exitance.

is presented for comparison in Fig. 7a. Figure 8 gives another illustration of exitance mapping; it contains a total exitance map for an apartment complex, together with a corresponding black-and-white infrared photograph.

Table 3 presents exitance values computed from multispectral scanner data for materials in the golf course scene (Fig. 7). The use of Eq. (11) for calculations for short-wavelength channels will now be described. Effective in-band exitance values, $M_{S_{cal}}$, were computed for each channel from the standard sources used to calibrate the scanner.* To obtain an effective lamp exitance value in band, each exitance value was divided by the voltage, $V_{S_{cal}}$, measured from the standard source at the time of calibration and multiplied by the reference lamp voltage, $V_{L_{cal}}$, measured at calibration. Then the term was multiplied by the lamp voltage, $V_{L_{data}}$, measured during data collection and divided by the lamp voltage, $V_{L_{cal}}$, for the same lamp current at the time of calibration. The result is an exitance response factor for each channel ($W \cdot cm^{-2}$/volt). To account for the spectral sampling of the scanner and atmosphere, each exitance response factor was multiplied by a spectral bandwidth scale factor, F_M. These scale factors were determined from calculated curves that represented (a) surface spectral exitance and (b) the product of surface spectral exitance and scanner relative spectral response functions. Each factor was calculated by first individually integrating (a) and (b) over a spectral interval that included the channel, and then forming the ratio $\int(a) \div \int(b)$. These spectral intervals were contiguous; thus the entire spectrum from 0.38 to 2.6 μm was approximated. The following equation summarizes the calculations employed to obtain the total exitance component measured by each channel:

$$M = \left[\left(\frac{M_{S_{cal}}}{V_{S_{cal}}}\right) V_{L_{cal}}\right]\left[\frac{V_{L_{data}}}{V_{L_{cal}}}\right]\left[F_M\right]\left[\frac{V_{data\ pt}}{V_{L_{data}}}\right] \tag{11}$$

The components are summed to obtain a total exitance contribution from the short-wavelength region.

Exitances in the thermal wavelength region are calculated in two steps because scene voltages in the thermal channel are measured by their magnitude in relation to signals from thermal reference sources in the scanner output, rather than in relation to a dark (no-radiance) level as are the other channels. For example, the difference between the scene voltage and the

*The effective exitance was assumed to be π times the effective radiance. Thus the reflectance of the surface viewed for calibration was assumed to be Lambertian.

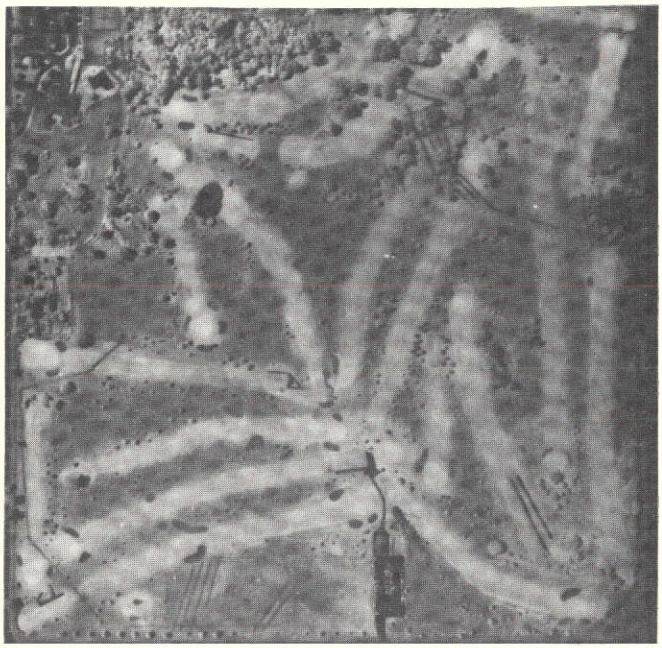

(a) B & W IR Photograph (6 Aug. 71, Alt = 5000 Ft, 9:57 EST, MSU)

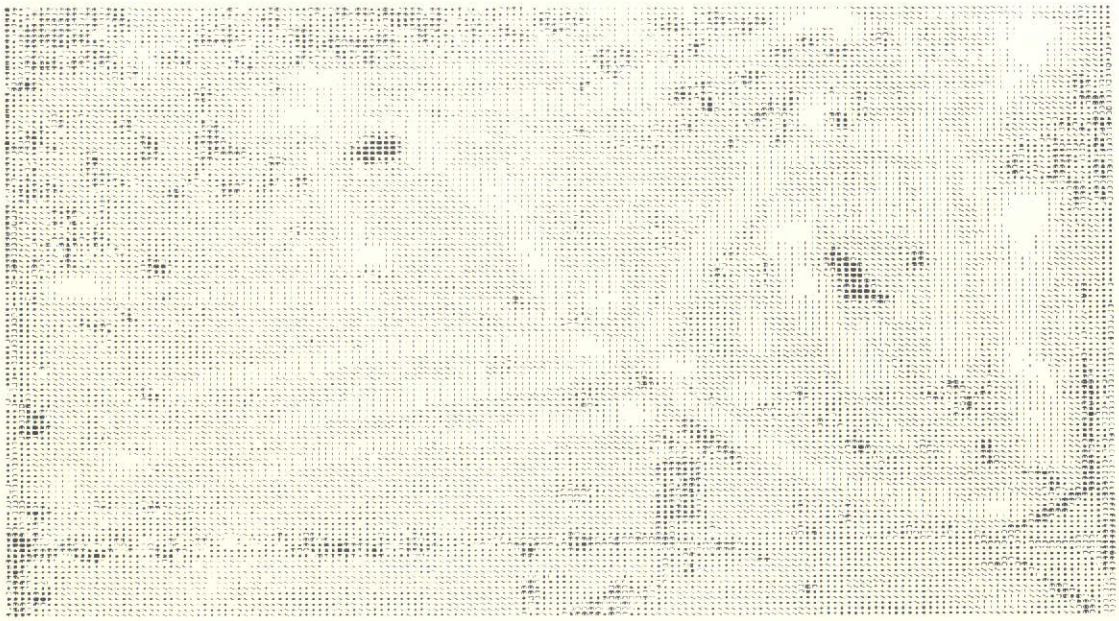

(b) Exitance Map (6 Aug. 71, Alt = 5000 Ft, 10:57 EST, MSU).
Light tones represent high values of total exitance.

FIGURE 7. GOLF COURSE

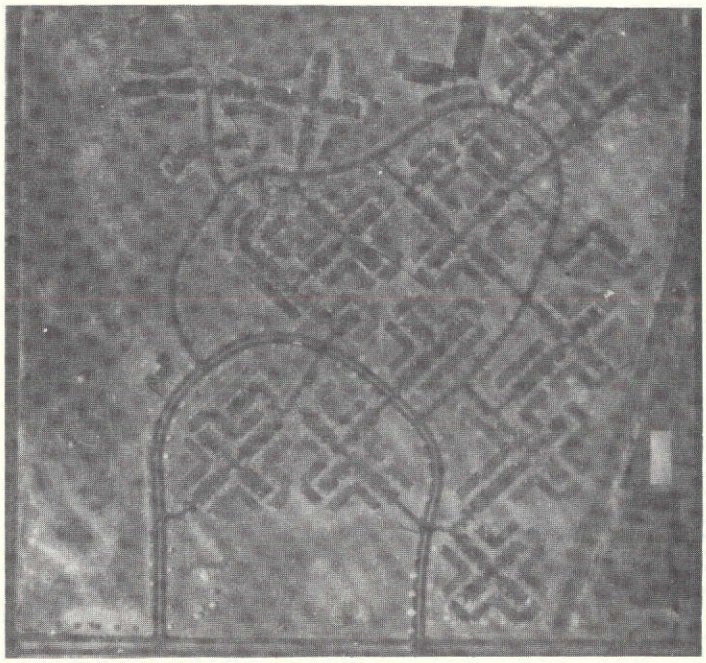

(a) B & W IR Photograph (6 Aug. 71, Alt = 5000 Ft, 9:57 EST, MSU)

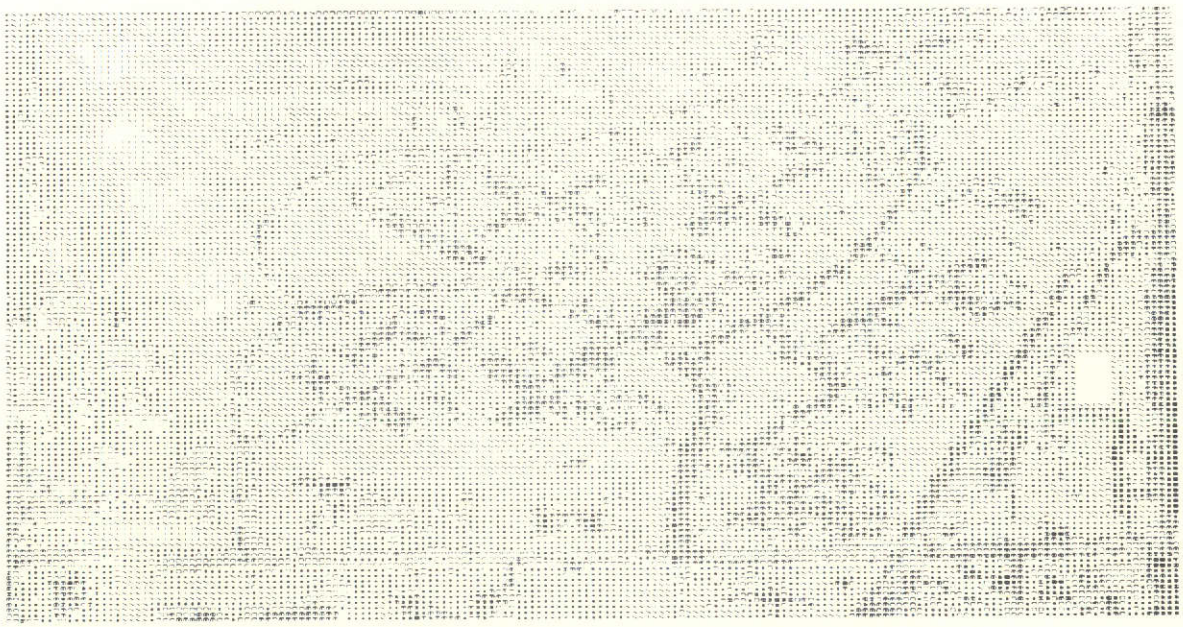

(b) Exitance Map (6 Aug. 71, Alt = 5000 Ft, 10:57 EST, MSU).
Light tones represent high values of total exitance.

FIGURE 8. APARTMENT COMPLEX

TABLE 3. EXAMPLE EXITANCE VALUES (COMPUTED FROM M-7 SCANNER DATA OF 8/06/71, 1057 HOURS, 5000 FT ALTITUDE)

EFFECTIVE (IN-BAND) VALUES FROM STANDARD SOURCE

CHNL NO.	50% RESPONSE WAVELENGTH SPAN (μm)	EXITANCE (W/m^2)	RADIANCE ($W/m^2 \cdot Sr$)	SPECTRAL RADIANCE $\left(\frac{mW}{cm^2 \cdot Sr \cdot \mu m}\right)$	SPECTRAL BANDWIDTH SCALE FACTOR (F_M)	DATA SET EXITANCE SCALE FACTOR* $\left(\frac{W/m^2}{volt}\right)$
1	.469-.486	0.554	0.176	1.04	4.0	16.1
2	.486-.506	0.766	.244	1.22	1.05	13.6
3	.508-.531	1.06	.338	1.47	1.13	7.9
4	.534-.560	1.45	.462	1.77	1.04	4.3
5	.560-.592	2.11	.672	2.10	1.00	11.4
6	.592-.626	2.63	.837	2.46	1.00	12.0
7	.630-.672	3.80	1.21	2.88	1.33	14.6
8	.694-.896	23.3	7.41	3.67	1.20	35.3
9	1.08-1.30	28.4	9.03	4.11	1.00	9.3
10	1.50-1.85	27.9	8.87	2.53	0.94	7.9
11	2.10-2.58	18.0	5.74	1.20	0.83	3.6
						Subtotal
12	9.3-11.7	(63.1= Exitance Scale Factor** for Thermal (emitted) data)				(Scene - Hot Plate) Exitance
						Hot Plate Thermal Exitance
						Total Exitance

EXITANCE VALUES COMPUTED FROM SCANNER DATA (in W/m^2)

GOLF GREEN	FAIRWAY	ROUGH	TREES	PARKING LOT	POND
21.40	20.80	25.63	16.80	31.04	20.48
8.17	8.02	9.99	6.00	11.15	7.40
12.12	11.18	12.51	7.96	13.14	9.83
16.22	14.76	14.45	10.07	13.46	12.48
16.93	15.71	17.06	10.45	15.51	14.26
12.08	11.90	15.48	7.58	13.93	10.39
12.57	13.87	21.72	8.07	17.67	13.07
292.13	251.80	168.62	198.39	82.37	107.9
91.07	84.62	60.08	65.06	28.90	22.51
36.58	33.05	38.67	23.47	16.15	7.85
8.28	8.20	10.04	5.68	5.42	2.94
528.6	473.91	394.25	359.55	248.74	229.11
1.1	-0.9	57.8	-31.42	52.06	-25.56
475.0	475.	475.	475.	475.	475.
1004.7	948.0	927.1	803.1	775.8	678.6

*Obtained for particular data set by measuring reference lamp voltages, using appropriate calibration data for the reference lamp current, and multiplying by the appropriate spectral bandwidth scale factors.

**Based on difference between total thermal exitances of hot and cold plates and corresponding voltage differential; thermal data were clamped to the hot plate value.

hot-reference voltage can be measured and then scaled by a ($W \cdot m^{-2}$/volt) factor obtained from voltages from the hot and cold reference sources and their known temperatures and exitances. The hot reference exitance is added to this differential exitance to obtain the total thermal exitance.

The total exitance is the sum of the short-wavelength and thermal exitance contributions. Next, upon estimating the incoming radiant power density at both short and long wavelengths, a map of apparent net radiation or radiation balance (that is, the total incoming radiant power density minus the total exitance) can be produced. Such a map would have the appearance shown in Fig. 9. Here, the relative tones are reversed from those in the exitance map of Fig. 6. For example, the wet soil and vegetation sites, which absorb the greatest net amount of radiation, are displayed in light tones. Also, the dirt/grass roadway across the center of the scene is dark, which indicates that most incident energy is either reflected or absorbed and re-radiated.

Finally, one could correct for atmospheric effects and estimate the energy budgets of the observed scene materials, that is, estimate the manner in which the net radiation is partitioned into the various components of the energy budget (Eq. 4). This step is more difficult than the preceding ones. It might be done on an instantaneous, or energy-rate, basis; or it might be done over an interval of time, in which case procedures would be required for estimating the time-integrated responses of the surface systems from the instantaneous remote sensor data. These types of information can be used for quantitative assessment of scene material conditions.

5.7. COMPUTER PROGRAM DEVELOPMENT

Three digital computer programs were developed for the CDC-1604 computer as a part of our investigation of radiation balance mapping techniques. While specific in origin, these computer programs are general in approach and have been adapted for other multispectral processing investigations and applications. The first, NET, simply produces a linear combination of scanner signals. Offset coefficients and weighting coefficients are included to permit conversion from voltage to radiance (or exitance) units and a separate term is included to convert relative radiance (or exitance values in the a-c coupled thermal channel to absolute values. In terms of exitance, the equation implemented is the same as Eq. (6):

$$E_{Net} = E_{Total} - A_1\left[\sum_{i=1}^{N} W_i(X_i - O_i) + M_{Ref}\right] \qquad (12)$$

where E_{Net} = the net incoming radiant power density

E_{Total} = the total incoming radiant power density for net exitance calculations

A_1 = a scaling factor

W_i = a weighting factor to convert scanner volts into exitance units for scanner channel i

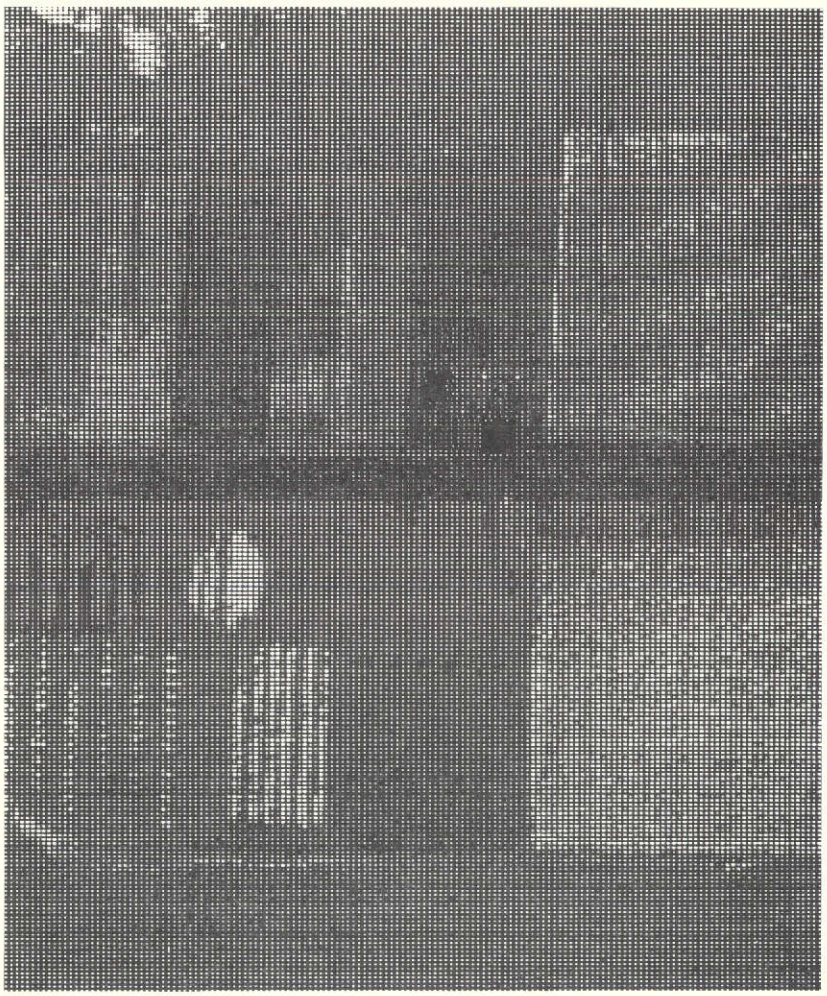

FIGURE 9. EXAMPLE RADIATION BALANCE MAP, AGRICULTURAL SITE (6 Aug. 71, Alt = 1000 Ft, 11:16 EST, MSU).
Light tones represent high positive values of net (absorbed) radiation.

X_i = the voltage signal in scanner channel i

O_i = an offset coefficient

M_{Ref} = the thermal exitance of the reference source used for the thermal data channel

Clearly, any consistent set of units can be used in the calculation of coefficients, scaling factors, and reference quantities.

The second computer program, RADMAP, has a two-channel output. The first channel contains a voltage level to represent the material class assigned by a multispectral recognition algorithm; the second channel contains a parameter of the input signals. In the case of RADMAP, the parameter in the second channel is a linear combination of signals of the type described in Eq. (12). In a later adaptation of this program at WRL, the second output channel has the probability density function exponent of the winning recognition signature, as evaluated at the scene point under consideration. Another feature of RADMAP is that it produces, for each recognition class of the first output channel, a histogram of those values put into the second output channel. Such histograms are useful in analyzing data and establishing limits for displaying data.

The third computer program, GRAY2, is a special program used to display information contained on a multiple-channel tape—such as the two-channel output tape of RADMAP. It produces a standard gray-map digital printout of data channel values for those resolution elements meeting specified criteria in the designated control channel. For example, one can map the exitance values for all scene elements recognized as corn by designating the recognition channel as the control channel and specifying those voltage level(s) that have been chosen to represent corn; there is also a feature that allows one to specify an interval in the control channel rather than a specific level or levels.

One segment (No. S212, M43) of 1970 Corn Blight Watch recognition data was studied by computing and printing a graymap of total exitance values for all resolution elements recognized as corn. This map was examined and several soybean areas that had been incorrectly called "corn" were found to have exitance values distinct from most true corn values and more like those for soybeans. This observation encourages further investigation of derived attributes in recognition processing.

6
CONCLUSIONS AND RECOMMENDATIONS

6.1. CONCLUSIONS

The availability of simultaneous registered multispectral data in reflective and thermal wavelengths presents problems for data analysis and processing as well as opportunities for increased information extraction.

A new, faster channel selection method that uses a linear approximation for computing probability of misclassification has been developed and implemented. Its use will provide a basis for making tradeoffs between processing cost and recognition performance in selecting the number of information channels to use for recognition processing.

Thermal data exhibit smaller scan angle effects than reflective data but are expected to be more sensitive to along-track and set-to-set variations. Calculations with a temperature prediction model demonstrated the lasting influence of cloud shadows on signals from bare soil. Evidence in the literature shows that vegetation responds much more rapidly and is less dependent on thermal history.

The use of multispectral scanner data for mapping exitance and radiation balance has been discussed as an initial step in the quantitative interpretation of physical and/or biological differences in scene materials through computer processing of remote sensor data. Example maps of apparent exitance and radiation balance have been presented for agricultural and urban applications; the results encourage further study of their use for assessing scene material conditions. Additional analysis is required to compensate for atmospheric effects, account for the bidirectional reflectance properties of surface materials, correlate the instantaneous remote sensor data with time-integrated phenomena, and evaluate energy budget components. The technique should be useful for other applications as well. Specialized computer programs were developed to generate and display the exitance and net radiation attributes derived from multispectral scanner data. Although specialized in application, these programs are general in concept and can be adapted to other uses.

6.2. RECOMMENDATIONS

Procedures for reducing the number of information channels by forming linear combinations of data channels should be investigated. Adoption of such procedures is expected to effect savings in recognition processing costs comparable to those realized through the use of channel subset selection procedures, with the advantage of a lesser performance penalty.

Additional investigations of exitance and radiation balance mapping procedures should be carried out. These and related procedures have potential for the extraction of information on scene material conditions for a variety of applications. In addition to identification of material classes, information on the conditions of scene materials is highly desired by users of area survey data. Other scene attributes derivable from multispectral scanner signals should also be considered.

Appendix

DERIVATION OF THE STEPLIN LINEAR CHANNEL SELECTION ALGORITHM

A common procedure for processing multispectral scanner data is to use only data contained in a selected subset of channels. We have found that this substantially decreases processing time without a significant increase in the average probability of misclassification.

Our method of selecting a subset of channels is fast, accurate, and computes an average probability of misclassification approximating the value that would be measured if the statistics of the data were known accurately. It was chosen after comparison with several alternative methods (see para. at end of this appendix), and an evaluation based on calculations of the average probability of misclassification for all possible subsets. An intuitive derivation of the method is now presented.

The average probability of misclassification is

$$\overline{P} = \sum_{i}^{K} p(H_i) \sum_{j \neq i} p(H_j | H_i) \tag{1}$$

where K is the number of classes to be recognized, $p(H_i)$ is the a priori probability of the class H_i being present, and $p(H_j | H_i)$ is the probability of choosing class H_j when class H_i is present. The usual method is to assume that the a priori probabilities are equal. In this case, Eq. (1) becomes

$$\overline{P} = \frac{1}{K} \sum_{j \neq i}^{K} p(H_j | H_i) \tag{2}$$

where the summation is over all ordered pairs of (i, j).

The first step in channel selection is to measure first and second order statistics (mean vectors and covariance matrices) of the training data. The assumption is made that the data are distributed normally, with all succeeding calculations of $\overline{P}$ based on this assumption.

All channels are tested individually to find the channel which, if used alone, would produce the minimum $\overline{P}$. The remaining channels are then tested together with the first channel selected, to find the combination that produces the minimum $\overline{P}$. This procedure is continued until all the channels are rank-ordered.

The calculation of the average probability of misclassification is based on several assumptions. The probability $p(H_j | H_i)$ is computed on a pairwise basis, ignoring the other classes and possible decisions. A linear discriminant is assumed, using a simplified method of cal-

culating its performance. Consider a pair of classes, say H_0 and H_1, both normal $N(\mu_0, R_0)$ and $N(\mu_i, R_i)$. Then one can show [29] that the optimum (in the Neyman-Pearson sense) linear decision rule is to say H_0 if

$$(x - \mu_0)^t R^{-1} \mu < q\mu^t R^{-1} R_0 R^{-1} \mu \tag{3}$$

with probabilities of misclassifications of Type I and Type II of

$$I = \phi\left[q(\mu^t R^{-1} R_0 R^{-1} \mu)^{1/2}\right] \quad = P[X \text{ classified as } \pi_1 \mid X \text{ in } \pi_0] \tag{4}$$

and

$$II = \phi\left[(1 - q)(\mu^t R^{-1} R_1 R^{-1} \mu)^{1/2}\right] \quad = P[X \text{ classified as } \pi_0 \mid X \text{ in } \pi_1] \tag{5}$$

where

$$R = qR_0 + (1 - q)R_1 \tag{6}$$

$$\mu = \mu_1 - \mu_0 \tag{7}$$

and

$$\phi(x) = \frac{1}{\sqrt{2\pi}} \int_x^\infty e^{-y^2/2} dy \tag{8}$$

The parameter q is chosen so that the average pairwise probability of misclassification, $(1/2)(I + II)$, is a minimum subject to the constraint that $0 \le q \le 1$. For channel selection we let $q = 1/2$ and use $(1/2)(R_0 + R_1)$ in place of R_0, R_1, R in Eqs. (4) and (5).

The channel selection procedure consists of using Eqs. (2), (4), and (5) with the simplification described in the previous paragraph. The channels are rank-ordered with an average probability of misclassification computed for each choice of the number of channels in the subset. The channels selected are the first n-ordered channels for a subset of size n. Accuracy in calculating average probability of misclassification depends upon how well the training data represent the remainder of the scene. However, it is possible to estimate the relative improvement that would occur from increasing the size of the subset.

Details of the calculations are as follows: With the substitutions noted above, Eqs. (4) and (5) become

$$I = II = \phi\left[1/2(\mu^t R^{-1} \mu)^{1/2}\right] \tag{9}$$

The equality of the Type I and II errors leads from Eq. (2) to the following expression for the average probability of misclassification

$$\overline{P} = \frac{2}{K}\sum_{i=1}^{K-1}\sum_{j=i+1}^{K} p(H_j|H_i) \tag{10}$$

To find the first channel, we form

$$\overline{P} = \frac{2}{K}\sum_{i=1}^{K-1}\sum_{j=i+1}^{K} \phi\left[(1/2)\frac{|\mu_{ik} - \mu_{jk}|}{(r_{kk})^{1/2}}\right] \tag{11}$$

for each channel, k, where

μ_{ik} = k-th component of i-th mean vector (of i-th material)

and

r_{kk} = kk element of R

where

$$R = (1/2)(R_i + R_j)$$

The first channel chosen is the one with the minimum $\overline{P}$.

The second channel is selected by computing

$$\overline{P} = (2/K)\sum_{i=1}^{K-1}\sum_{j=1}^{K}\phi\left\{(1/2)\left[\begin{pmatrix}\mu_{ik} - \mu_{jk}\\ \mu_{i\ell} - \mu_{j\ell}\end{pmatrix}^t\begin{pmatrix}r_{kk} r_{k\ell}\\ r_{\ell k} r_{\ell\ell}\end{pmatrix}^{-1}\begin{pmatrix}\mu_{ik} - \mu_{jk}\\ \mu_{i\ell} - \mu_{j\ell}\end{pmatrix}\right]^{1/2}\right\} \tag{12}$$

using for k the first channel selected and, for ℓ, all channels except the first channel selected. The second channel becomes that value of ℓ for which Eq. (12) is a minimum. Of course, the average probability of misclassification becomes that minimum. This procedure is continued until all channels are ordered and an average probability of misclassification is found for each size of subset.

This algorithm was chosen after a comparison with two other linear algorithms for seven pairs of signatures. Quadratic calculations with the STEPER2 algorithm were used as the standard for judging the accuracy of probability of misclassification estimates. The first linear alternative was that of searching for the value, q, that minimizes the sum of Type I and Type II errors (Eqs. 4 and 5). The second alternative was to assume q = 1/2 and evaluate Eqs. (4) and (5) using the two covariance matrices R_0 and R_1. The results obtained were no better than those obtained with the selected algorithm and the computation times were longer. Actually, the different methods did not rank all of the subsets in the same way, but the computed differences in performances for equally ranked subsets, obtained by using different methods, was insignificant.

REFERENCES

1. Manual of Photographic Interpretation, American Society of Photogrammetry, Washington, D.C., 1960.

2. Braithwaite, J. G. N., "Airborne Multispectral Sensing and Applications," J. Soc. Photo-Opt. Instrumentation Engr., Vol. 8, No. 4, April-May 1970, pp. 139-144.

3. Hasell, P. G., Jr., "Michigan Experimental Scanner System," 4th Annual Earth Resources Program Review, Jan. 1972, at NASA/MSC, Houston, MSC-05937, Vol. II.

4. Malila, W. A., R. B. Crane, W. Richardson, and R. E. Turner, "Information Extraction Techniques for Multispectral Scanner Data," 4th Annual Earth Resources Program Review, Jan. 1972, at NASA/MSC, Houston, MSC-05937, Vol. II.

5. Crane, R. B. and W. Richardson, "Rapid Processing of Multispectral Scanner Data Using Linear Techniques," in Remote Sensing of Earth Resources, Vol. I, ed. by F. Shahrokhi, University of Tennessee Space Institute, Tullahoma, Tenn., 1972.

6. Crane, R. B., W. Richardson, R. H. Hieber, and W. A. Malila, "A Study of Techniques for Processing Multispectral Scanner Data," Environmental Research Institute of Michigan, Ann Arbor, Report NASA CR ERIM 31650-155-T, September 1973.

7. Vincent, R. K., "Experimental Methods for Geological Remote Sensing," 4th Annual Earth Resources Program Review, Jan. 1972, at NASA/MSC, Houston, MSC-05937, Vol. II.

8a. Nalepka, R. F., J. P. Morgenstern, and W. L. Brown, "Detailed Interpretation and Analysis of Selected Corn Blight Watch Data Sets," 4th Annual Earth Resources Program Review, Jan. 1972 at NASA/MSC, Houston, MSC-05937, Vol. V.

8b. 1971 Corn Blight Watch Experiment Final Report, Vol. III, Experiment Results, Purdue University Laboratory for Applications of Remote Sensing (LARS) [in press].

9. Loomis, Walter E., "Absorption of Radiant Energy by Leaves," Ecology, Vol. 46, No. 1, pp. 14-16, 1965.

10. Gates, David M., "Energy, Plants, and Ecology," Ecology, Vol. 46, Nos. 1 and 2, 1965.

11. Horvath, R., "Thermal Modeling for Mission Planning and Data Analysis," in Remote Sensing Analysis Projects—NASA, Report 31650-26-T, Willow Run Laboratories, The University of Michigan, Ann Arbor, 1971.

12. Sellers, William D., Physical Climatology, University of Chicago Press, 1965.

13. Gates, David M., Energy Exchange in the Biosphere, Harper and Row, New York, 1962.

14. Turner, R. E., and W. A. Malila, and R. F. Nalepka, "Importance of Atmospheric Scattering in Remote Sensing," Proceedings of Seventh International Symposium on Remote Sensing of Environment, 17-21 May 1971, Willow Run Laboratories, The University of Michigan, Ann Arbor.

15. Rose, H. M., D. C. Anding, and J. Walker, "Computation of Atmospheric Effects on Remote Sensing," Proceedings of Seventh International Symposium on Remote Sensing of Environment, 17-21 May 1971, at Willow Run Laboratories, The University of Michigan, Ann Arbor.

16. Malila, W. A., "Multispectral Techniques for Image Enhancement and Discrimination," Photogrammetric Engineering, Vol. XXXIV: 566-575, 1968.

17. Raschke, E. and W. R. Bandeen, "The Radiation Balance of the Planet Earth from Radiation Measurements of the Satellite Nimbus II," J. Appl. Meteor., 9:215-237, 1970.

18. Suits, G. H., "Calculation of the Directional Reflectance of a Vegetative Canopy," Remote Sensing of Environment, American Elsevier, New York, Vol. 2, No. 2, 1972.

19. Horvath, R. and W. L. Brown, "Multispectral Radiative Characteristics of Arctic Sea Ice and Tundra." Report No. 27980-2-F, Willow Run Laboratories, Institute of Science and Technology, The University of Michigan, Ann Arbor, 1971.

20. Malila, W. A., "Radiation Balance Mapping with Multispectral Scanner Data," in Remote Sensing of Earth Resources, Vol. I, ed. by F. Shahrokhi, University of Tennessee Space Institute, Tullahoma, Tenn., 1972.

21. Griggs, M., "Aircraft Measurements of Albedo and Absorption of Stratus Clouds, and Surface Albedos," J. Appl. Meteor., 7:1012-1017, 1968.

22. Malila, W. A., and T. W. Wagner, "Multispectral Remote Sensing of Elements of Water and Radiation Balances" Proceedings of 8th International Symposium on Remote Sensing of Environment, 2-6 Oct. 1972, at Willow Run Laboratories, The University of Michigan, Ann Arbor.

23. Thornthwaite, C. Warren and F. Kenneth Hare, "The Loss of Water to the Air," Meteorological Monographs, Chap. 11, 1965.

24. Tanner, C. B., "Evaporation of Water From Plants and Soil," Water Deficits and Plant Growth, Vol. I, ed. by T. T. Kozlowski, Academic Press, New York, 1968.

25. Wiegand, C. L., M. D. Heilman, and A. H. Gerberman, "Detailed Plant and Soil Thermal Regime in Agronomy," Proceedings of Fifth Symposium on Remote Sensing of Environment, 16-18 April 1968, at Willow Run Laboratories, The University of Michigan, Ann Arbor.

26. Tanner, C. B. and W. L. Pelton, "Potential Evapotranspiration Estimates by the Approximate Energy Balance Method of Penman," J. Geophys. Res., 64:3391-3413, 1960.

27. Van Bavel, C. H. M., "Potential Evaporation: The Combination Concept and Its Experimental Verification," Water Resources Res., Vol. 2, No. 2, pp. 455-467, 1966.

28. Penman, H. L., "Natural Evaporation From Open Water, Bare Soil and Grass," Proc. Roy. Soc. (London), 193, A, 120-145, 1968.

29. Anderson, T. W. and R. R. Bahadur, "Classification into Two Multivariate Normal Distributions with Different Covariance Matrices," Annals of Mathematical Statistics, Vol. 33, pp. 420-431, 1962.

30. Leeman, V., D. Earing, R. Vincent, and S. Ladd, "The NASA Earth Resources Spectral Information System: A Data Compilation," Report No. NASA CR WRL-31650-24-T, Willow Run Laboratories, The University of Michigan, Ann Arbor, Mich., May 1971.